U.S. DEPARTMENT OF ENERGY | Office of Science

UM-ASU Final Report

Assessing the Role of Iron Sulfides in the Long Term Sequestration of Uranium by Sulfate-Reducing Bacteria

Kim F. Hayes (PI), Yuqiang Bi, Julian Carpenter, and Sung Pil Hyun
University of Michigan
Bruce E. Rittmann (co-PI), Chen Zhou, Raveender Vannela
Arizona State University
James A. Davis (co-I)
LBNL

Executive Summary

This four-year project's overarching aim was to identify the role of biogenic and synthetic iron-sulfide minerals in the long-term sequestration of reduced U(IV) formed under sulfate-reducing conditions when subjected to re-oxidizing conditions. As stated in this final report, significant progress was achieved through the collaborative research effort conducted at Arizona State University (ASU) and the University of Michigan (UM).

Research at ASU, focused on the biogenesis aspects, examined the biogeochemical bases for iron-sulfide production by *Desulfovibrio vulgaris*, a Gram-negative bacterium that is one of the most-studied strains of sulfate-reducing bacteria. A series of experimental studies were performed to investigate comprehensively important metabolic and environmental factors that affect the rates of sulfate reduction and iron-sulfide precipitation, the mineralogical characteristics of the iron sulfides, and how uranium is reduced or co-reduced by *D. vulagaris*. As discussed in Section 2 of this report, the FeS production studies revealed that controlling the pH -- by varying the initial pH, the iron-to-sulfate ratio, or the electron donor --, affected the growth of *D. vulgaris* and strongly influenced the formation and growth of FeS solids. In particular, lower pH (from initial conditions or a decrease caused by less sulfate reduction, FeS precipitation, or using pyruvate as the electron donor) produced larger-sized mackinawite ($Fe_{1+x}S$). Greater accumulation of free sulfide, from more sulfate reduction by *D. vulgaris,* also led to larger-sized mackinawite and stimulated mackinawite transformation to greigite (Fe_3S_4) when the free sulfide concentration was 29.3 mM. On the other hand, using solid Fe(III) (hydr)oxides as the iron source led to less productivity of FeS due to their slow and incomplete dissolution and scavenging of sulfide. Furthermore, sufficient free Fe^{2+}, particularly during Fe(III) (hydr)oxide reductions, led to the additional formation of

vivianite [$Fe_3(PO_4)_2 \cdot 8(H_2O)$]. The U(VI) reduction studies revealed that *D. vulgaris* reduced U(VI) fastest when accumulating sulfide from concomitant sulfate reduction, since direct enzymatic and sulfide-based reductions of U(VI) occurred in parallel. The UO_2 produced in presence of ferrous iron was poorly crystalline.

At UM, laboratory-scale reactor studies were performed to assess the potential for the predominant abiotic reductants formed under sulfate reducing conditions (SRCs) to: (1) reduce U(VI) in contaminated groundwater sediments), and (2) inhibit the re-oxidation of U(IV) species, and in particular, uraninite ($UO_2(s)$). Under SRCs, mackinawite and aqueous sulfide are the key reductants expected to form. The former, when sediments contain significant amounts of Fe, and the later as a result of sulfate reduction. To assess their potential for abiotic reduction of U(VI) species, a series of experiments were performed in which either FeS or S(-II) was added to solutions of U(VI), with the rates of conversion to U(IV) solids monitored as a function of pH, and carbonate and calcium concentration (Section 3). In the presence of FeS and absence of oxygen or carbonate, U(IV) was completely reduced uraninite. S(-II) was also found to be an effective reductant of aqueous phase U(VI) species and produced uraninite, with the kinetics and extent of reduction depending on geochemical conditions. U(VI) reduction to uraninite was faster under higher S(-II) concentrations but was slowed by an increase in the dissolved Ca or carbonate concentration. Rapid reduction of U(VI) occurred at circumneutral pH but virtually no reduction occurred at pH 10.7. In general, dissolved Ca and carbonate slowed abiotic U(VI) reduction by forming stable Ca-U(VI)-carbonate soluble complexes that are resistant to reaction with aqueous sulfide.

To investigate the stability of U(IV) against re-oxidation in the presence of iron sulfides by oxidants in simulated groundwater environments, and to develop a mechanistic understanding the controlling redox processes, continuously-mixed batch reactor (CMBR) and flow-through reactor (CMFR) studies were performed at UM

(Section 4). In these studies a series of experiments were conducted under various oxic groundwater conditions to examine the effectiveness of FeS as an oxygen scavenger to retard UO_2 dissolution. The results indicate that FeS is an effective oxygen scavenger, and can lower the rate of oxidative dissolution of UO_2 by over an order of magnitude compared to the absence of FeS, depending on pH, FeS content, and DO concentrations. Compared to oxygen as an oxidant, the results also indicate that Fe(III) products of FeS oxidation (e.g., lepidocrocite or goethite), have a negligible impact on oxidative dissolution of uraninite when oxygen is present (e.g., when DO concentrations are >0.5 mg/L).

Column reactor studies were performed at UM to assess the impact of mackinawite on uraninite oxidation under hydrodynamic flow conditions more representative of packed porous media at contaminated groundwater sites (Section 5). In these studies, Rifle sediments were packed in the two columns which were subjected to different bioreduction steps and then run in parallel. The first column was bioreduced under SRCs (i.e., with sulfate in the influent) to generate mackinawite, mixed with uraninite, gamma-sterilized to inhibit subsequent microbiological activity, and then subjected to groundwater influent containing first nitrite and then oxygen. The second column was bioreduced (but in absence of sulfate in the influent) so that no iron sulfides would form, and then subjected to identical steps and influent as the first column. When nitrite was introduced in the influent of both columns, no significant release of U(VI) relative to the anoxic flow prior to nitrite addition occurred. However, when oxygen was introduced, the column which had undergone sulfate reduction (and had produced mackinawite as later verified by XAS) significantly lowered the peak U(VI) effluent concentrations, and in general, slowed U(VI) release considerably compared to the column with no FeS. Overall, these studies demonstrated that the presence of mackinawite can be a significant

scavenger of oxygen and inhibit the oxidation of uraninite by oxygen, whereas nitrite had little impact on uraninite oxidation either in the presence or absence of FeS.

The results of these studies have resulted in 10 peer-reviewed journal manuscripts (either currently published, in review, or submitted) and 18 presentations at National, International, or Internal venues (see Section 6).

Table of Contents

1. Overall Project Description

As a result of nuclear fuel production, weapons manufacturing, and research activities, uranium (U) is one of the most prevalent radionuclide contaminants in soils and groundwater across the world. Aqueous U(VI) concentrations in groundwater can be effectively lowered by reducing dissolved U(VI) species to insoluble U(IV) solids such as uraninite ($UO_2(s)$). During active bioremediation, sulfate reducing bacteria (SRB) can reduce aqueous-phase U(VI) to insoluble UO_2 through enzymatic electron transfer processes or indirectly through chemical reduction by the biogenic sulfide species. Naturally occurring iron sulfide minerals (FeS) can also supply electrons for abiotic uranium reduction in biostimulated aquifers. The close association of UO_2 with FeS found in the field suggests that FeS may serve as an effective redox buffer for long-term U stabilization in subsurface environments. Upon oxidant intrusion, FeS may inhibit reoxidation of reduced U solid phases formed during a reductive bioremediation phase. Understanding the role of FeS in protecting UO_2 against reoxidation is important for assessing the long-term stability of bioreduced U-contaminated aquifers.

This collaborative research was aimed at identifying the role of biogenic and synthetic iron-sulfide minerals in the long-term sequestration of uranium (U) in the presence of sulfate-reducing bacteria (SRB). Specifically, Arizona State University (ASU) research focused on the formation of iron-sulfide and uraninite solids by SRB and how growth conditions affected the rate and characteristics of the solids. The University of Michigan (UM) research evaluated the ability of the biogenic and synthetic iron-sulfide solids to inhibit the oxidation and solubilization of UO_2.

This final report summarizes the experimental results of the microbial, chemical, and spectroscopic research that the collaborative team carried out with iron sulfides and reduced U(IV) over the past four years. The report includes 5 Sections that cover the major scientific findings.   Most of the results are reported in journal publications and

conference presentation, which are summarized in the publication list at the end of the report in Section 6. The over-arching goals of this research were to gain fundamental, mechanistic understanding from a series of experimental studies and to assess the potential for iron sulfides created under sulfate reducing conditions to inhibit U(IV) remobilization and the stability of U in the subsurface against re-oxidation by oxidants such as oxygen and nitrite.

2. Biogenic iron-sulfide and uraninite solids by *Desulfovibrio vulgaris*

Research at ASU focused on the biogenesis aspect and examined the biogeochemical bases for iron-sulfide production by *Desulfovibrio vulgaris*, a Gram-negative bacterium that is one of the most-studied strains of SRB. *D. vulgaris* gains energy from either organic or inorganic electron donors while respiring sulfate, as well as various metals (e.g., U, Fe, and Cr). Its biogenic products, like hydrogen sulfide and iron sulfide, have the potential to chemically reduce U(VI), as well as to inhibit uraninite re-oxidation by oxygen, nitrate, and Fe(III) (Abdelouas et al., 1999a). Thus, *D. vulgaris* was an ideal model bacterium for gaining deep insights into what controls the quantity and quality of biogenic iron sulfides.

The ASU team performed a series of experimental studies that looked comprehensively at important metabolic and environmental factors that affect the rates of sulfate reduction and iron-sulfide precipitation, the mineralogical characteristics of the iron sulfides, and how uranium is reduced or co-reduced by *D. vulagaris*. In the following sections, we present the ASU results in three sections that correspond to journal manuscripts that we have submitted for publication or will submit soon. They address (1) the role of growth conditions (e.g., electron donor, pH, iron concentration) on iron-sulfide formation and characteristics, (2) the role of the iron source on iron-sulfide formation and characteristics, and (3) the co-reduction of uranium and sulfate. In each section, we highlight the most important results by presenting a condensed version of the journal manuscript.

2.1 Effect of growth conditions on formation and characteristics of biogenic iron-sulfide solids by Desulfovibrio vulgaris

In the first study, the growth, metabolism, and FeS production of *D. vulgaris* were comprehensively evaluated in batch studies, and the biogenic FeS solids were

characterized by X-ray diffraction (XRD). We varied the concentration and type of electron donor, the pH, and the concentration of iron.

*Lactate-to-*sulfate *mole ratio.* We tested three different lactate-to-sulfate mole ratios (0.5:1, 0.8:1, and 1.9:1) by changing lactate concentrations in the original ATCC medium. By fermenting lactate, *D. vulgaris* produced H_2 to provide electrons for sulfate reduction to sulfide, which led to the formation of crystalline mackinawite when Fe^{2+} was present. As shown in the left side of Figure 2.1, the similar growth rates of *D. vulgaris* with different lactate concentrations suggest that the half-maximum rate concentration (K_s) of lactate was small for *D. vulgaris*, and, thus, high lactate-to-sulfate ratios did not affect the kinetics of bacterial growth. However, higher lactate-to-sulfate ratios enhanced FeS crystallization (shown by XRD patterns in the right side of Figure 2.1) by producing more sulfide from sulfate reduction. In particular, the highest lactate-sulfate mole ratio (1.9:1) led to the presence of greigite, which normally forms slowly via the reaction of mackinawite with aqueous H_2S or polysulfides (Wilkin and Barnes, 1996; Wilkin and Barnes, 1997; Herbert et al., 1998).
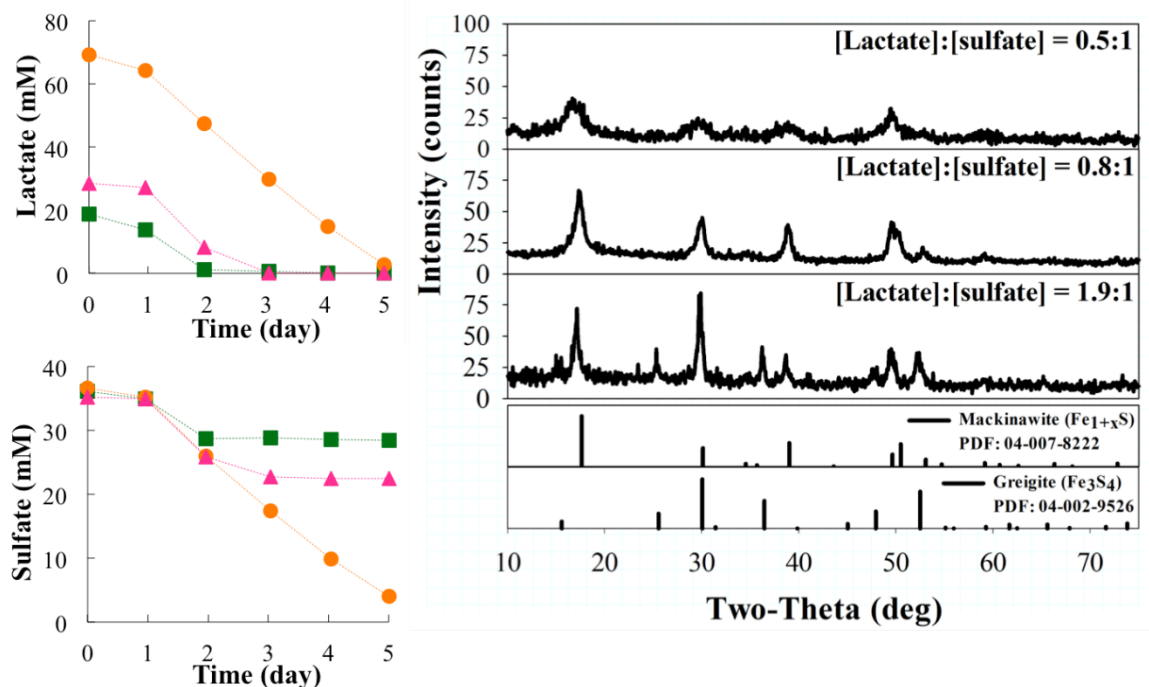
Figure 2.1. Lactate (left top) and sulfate (left bottom) during the growth of *D. vulgaris* with initial lactate-to-sulfate mole ratios of 0.5:1 (●), 0.8:1 (▲), and 1.9:1 (■); XRD patterns of solids separated from these *D. vulgaris* cultures (right).

Iron-to-sulfate ratio. We tested four different iron-to-sulfate mole ratios (0.11:1, 0.25:1, 0.5:1, and 0.9:1) by increasing the soluble Fe^{2+} concentrations in the original ATCC medium. Figure 2.2 summarizes the results. Varying the iron-to-sulfate ratio showed that an initial soluble Fe^{2+} concentration as high as 30 mM did not inhibit bacterial growth. However, higher initial soluble Fe^{2+} concentration led to lower initial and final pHs, which probably caused the slightly slower growth (left side of Figure 2.2). Moreover, the XRD patterns in the right side of Figure 2.2 show that mackinawite was present in all solid samples generated from the various iron-to-sulfate ratios. Higher iron concentration enhanced the process of crystallite growth of mackinawite, probably by accelerating the rate of FeS formation. In particular, the highest initial iron-to-sulfate mole ratio (0.9:1) consumed all free sulfide to form iron-sulfide, leaving a considerable residual of dissolved Fe(II) (14.0 mM). Sufficient dissolved Fe(II) and absence of the inhibitive sulfide resulted in formation of vivianite [$Fe_3(PO_4)_2 \cdot 8(H_2O)$].
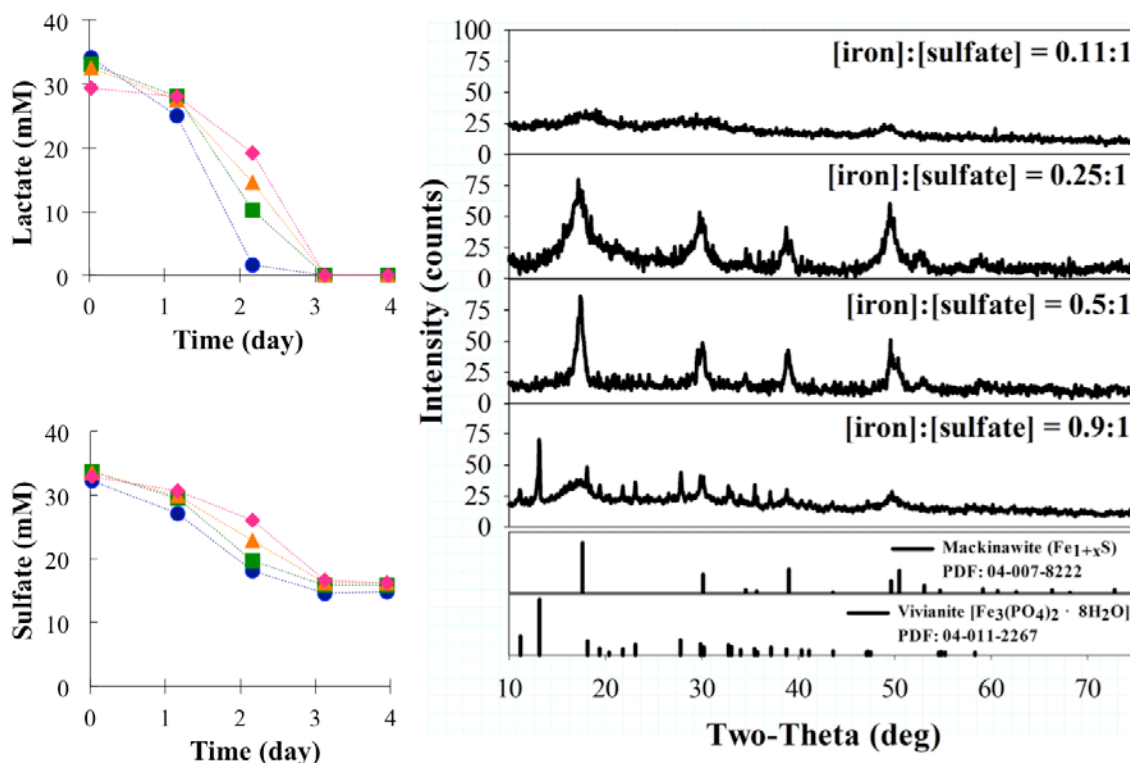
Figure 2.2. Lactate (left top) and sulfate (left bottom) during the growth of *D. vulgaris* with initial iron-to-sulfate mole ratios of 0.11:1 (●), 0.25:1 (■), 0.5:1 (▲), and 0.9:1 (◆); XRD patterns of solids separated from these *D. vulgaris* cultures (right).

pH value. We tested five different initial pH values: 5.6, 6.5, 6.9, 7.3, and 8.6. As shown by the left side of Figure 2.3, a favorable environment for *D. vulgaris* was circumneutral pH (6.5 – 7.3). Bacterial growth was considerably retarded at initial pH values of 5.6 and 8.9 over eight days, although *D. vulgaris* eventually adapted. The quantity of solids produced for the initial pH of 5.6 was negligible, but the right side of Figure 2.3 shows that the other pH values gave distinctive XRD patterns, although all corresponded to mackinawite. This suggests that the rate of mackinawite crystal growth was quite sensitive to pH, with lower pH leading to more crystalline mackinawite.
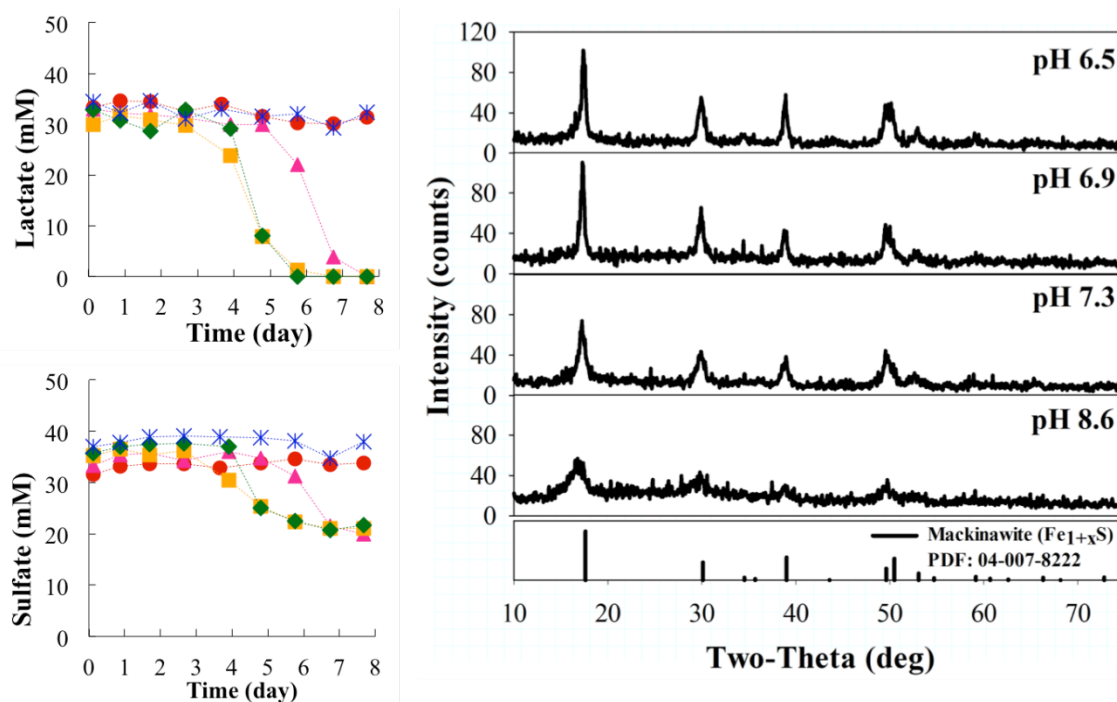
Figure 2.3. Lactate (left top) and sulfate (left bottom) during the growth of *D. vulgaris* with initial pHs of 5.6 (●), 6.5 (▲), 6.9 (■), 7.3 (◆) and 8.6 (*) within 8 days; XRD patterns of solids separated from the *D. vulgaris* cultures with various initial pHs (right).

Electron donors. Besides lactate, we also tested two other electron donors (pyruvate and H_2 gas) by replacing lactate in the original ATCC medium. Results are summarized in Figure 2.4. *D. vulgaris* grown with pyruvate or hydrogen gas had faster utilization rates than lactate (left side of Figure 2.4), because pyruvate is the first intermediate during lactate fermentation to acetate, while H_2 is the product of lactate or pyruvate fermentation as well as the ultimate electron carrier responsible for sulfate reduction (Voordouw, 2002; Heidelberg et al., 2004). Mackinawite produced from H_2 gas was slightly less crystalline (right side of Figure 2.4), because H_2 oxidation by *D. vulgaris* increased the pH; in contrast, considerably more crystalline mackinawite was produced from pyruvate because pyruvate fermentation by *D. vulgaris* decreased the pH. This trend corresponds to our previous pH results and underscores that the FeS-crystallization process was affected more by the pH than by the electron donor type.
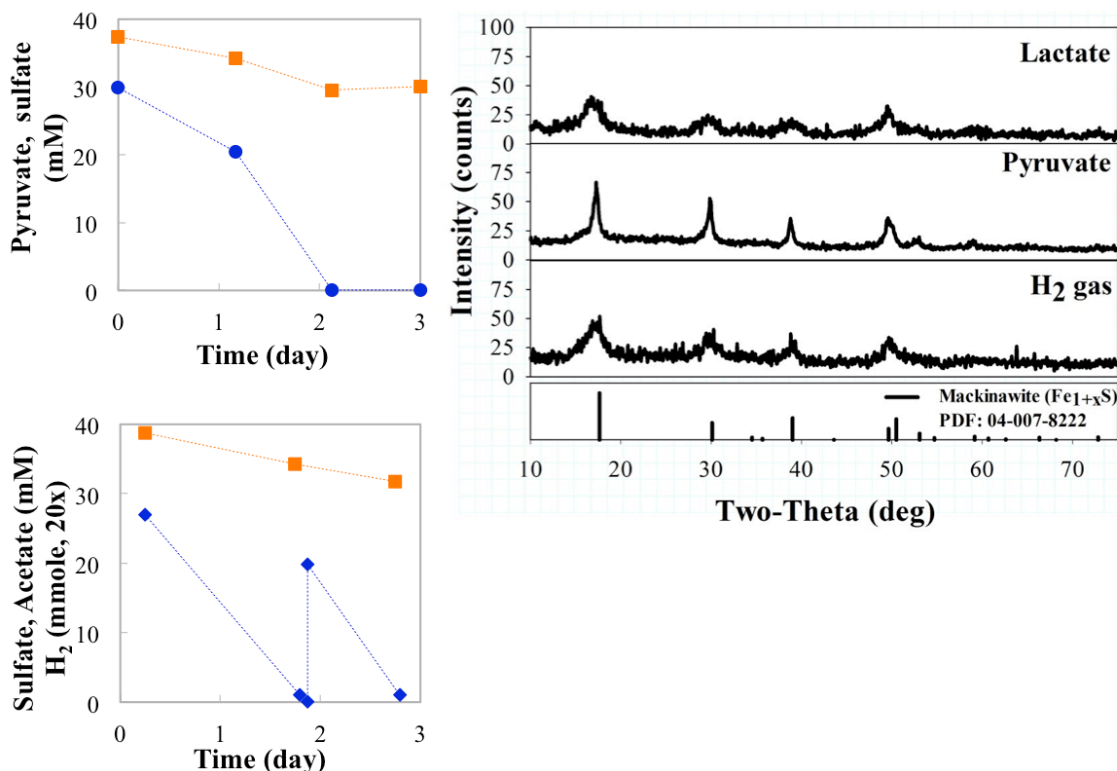
Figure 2.4. Pyruvate ($\bullet$) and sulfate ($\blacksquare$) in the culture of *D. vulgaris* growing exclusively on pyruvate (left top); H_2 ($\blacklozenge$) and sulfate ($\blacksquare$) in the culture of *D. vulgaris* growing exclusively on hydrogen gas (left bottom); XRD patterns of solids separated from the *D. vulgaris* cultures with different electron donors (right).

In summary for this section, we revealed that pH, soluble Fe^{2+} concentration, and free sulfide concentration were key factors affecting *D. vulgaris* growth and FeS production. Higher soluble Fe^{2+} and lower pH slightly retarded bacterial growth, but, along with higher free sulfide, considerably enhanced the formation of more-crystalline mackinawite. Thus, a growth condition of low electron-donor-to-sulfate mole ratio (for less free sulfide), lower soluble Fe^{2+}, slightly alkaline pH, and an electron donor producing less protons may be beneficial to form more-amorphous biogenic iron-sulfide, which we anticipate will have higher activity for uranium sequestration.

2.2 Effect of iron source on formation and characteristics of biogenic iron-sulfide solids by Desulfovibrio vulgaris

The iron source is believed to have an impact on the formation rate and characteristics of biogenic iron-sulfide solids (Sani et al., 2004; Li et al., 2006). In the second study, we applied a range of iron sources, including soluble Fe(II) and Fe(III) and three different Fe(III) (hydr)oxides. We evaluated sulfate reduction kinetics, FeS production, and FeS characteristics with lactate or pyruvate as the electron donor.

Soluble iron sources: Fe^{2+} and Fe^{3+}. In the tests with $FeCl_2$ as the soluble iron source, sulfate was the sole electron acceptor. As shown in Figure 2.5, sulfate reduction was slightly faster when pyruvate was the electron donor, indicating that lactate fermentation to pyruvate is the limiting step during the entire process of lactate fermentation.   Soluble Fe^{2+} decreased alongside sulfate reduction, indicating the formation of FeS precipitates from biogenic sulfide. In the tests with $FeCl_3$, soluble Fe^{3+} was as an additional electron acceptor; soluble Fe^{3+} was a more favorable acceptor than sulfate due to its higher redox potential, and its reduction inhibited sulfate reduction. When lactate was the electron donor, sulfate reduction did not start until all Fe^{3+} was reduced to Fe^{2+}.   When pyruvate was the electron donor, sulfate reduction was considerably retarded, but not completely inhibited when Fe^{3+} was being reduced to Fe^{2+}.

As shown in Figure 2.6, the different patterns of sulfate reduction had great impacts on FeS formation. Retarding sulfate reduction and, thus, sulfide production allowed for temporary accumulation of soluble Fe^{2+} in the medium, and it also delayed FeS formation. Significantly more crystalline mackinawite was produced with soluble Fe^{2+}, probably due to the earlier formation of FeS and the longer period for subsequent crystallization. In addition, the mackinawite was better crystallized with pyruvate than with lactate due to a lower pH during pyruvate fermentation. This is in consistent with the observations in our previous experiments.
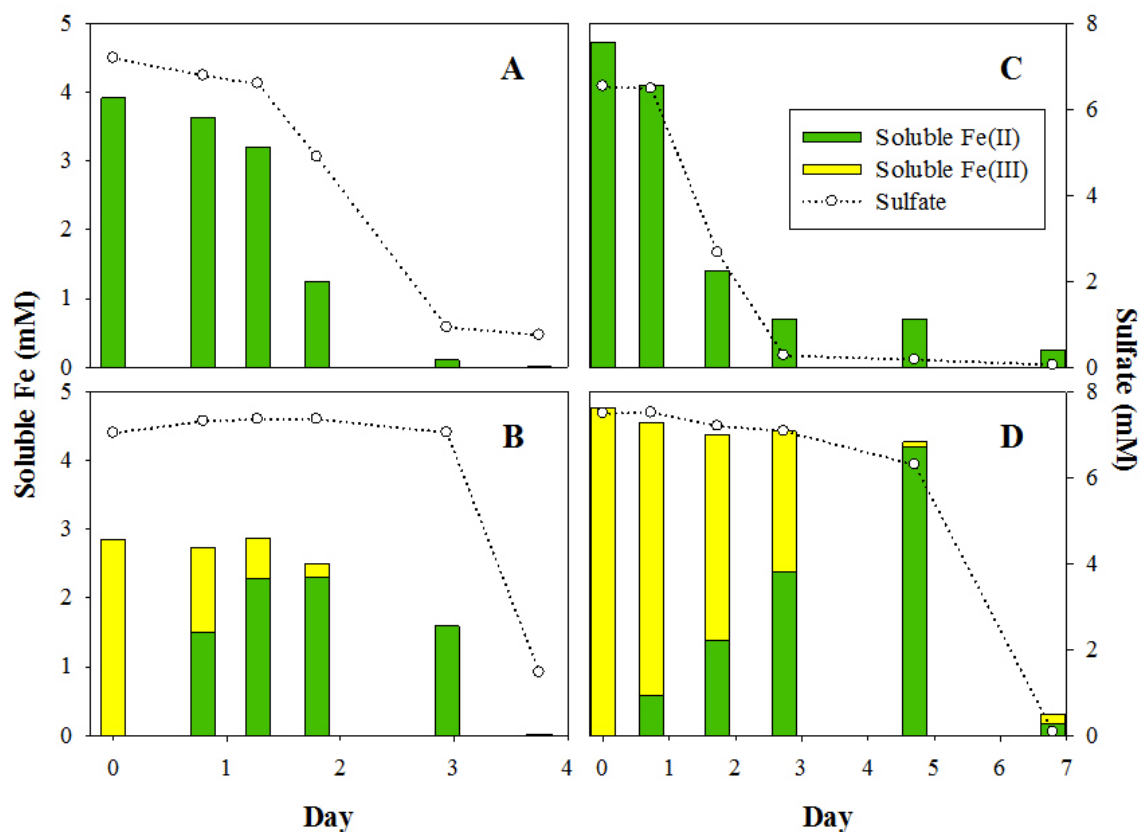
Figure 2.5. Concentrations of soluble Fe(II) (—), soluble Fe(III) (—) and sulfate (○) during the growth of *D. vulgaris* with lactate as the electron donor plus soluble Fe^{2+} as the iron source (A), lactate as the electron donor plus soluble Fe^{3+} as the iron source (B), pyruvate as the electron donor plus soluble Fe^{2+} as the iron source (C), and pyruvate as the electron donor plus soluble Fe^{3+} as the iron source (D).
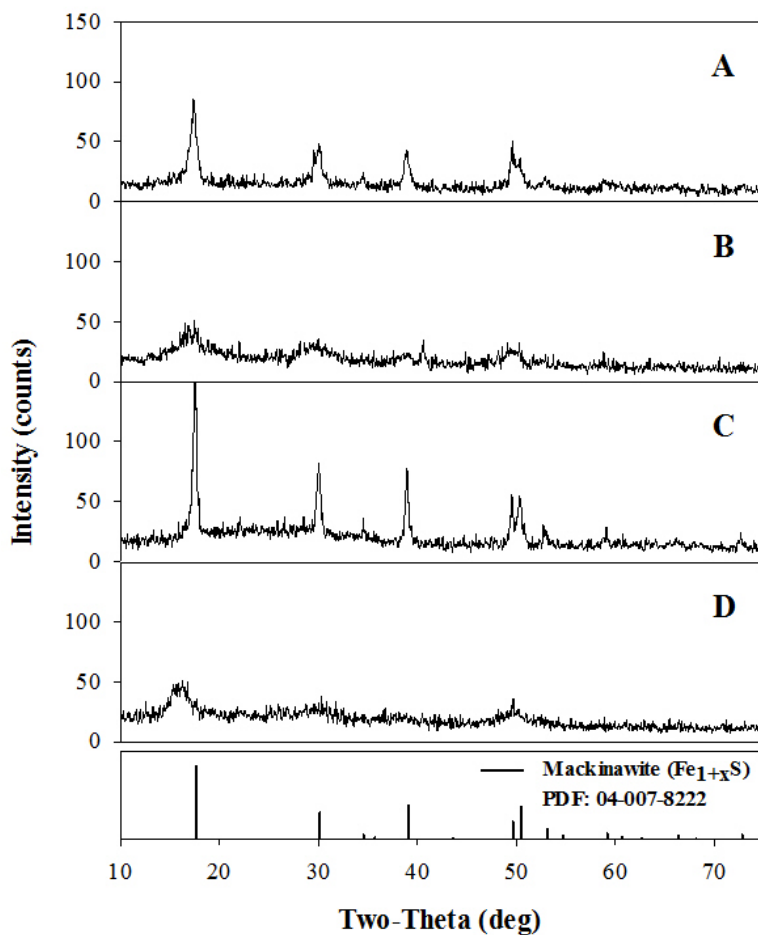
Figure 2.6. XRD spectra of solids separated from media with lactate as the electron donor plus soluble Fe^{2+} as the iron source (A), lactate as the electron donor plus soluble Fe^{3+} as the iron source (B), pyruvate as the electron donor plus soluble Fe^{2+} as the iron source (C), and pyruvate as the electron donor plus soluble Fe^{3+} as the iron source (D).

Solid iron sources: Fe(III) (hydr)oxides. We synthesized three Fe(III) (hydr)oxides: goethite (α-FeOOH), hematite (α-Fe_2O_3), and 2-line ferrihydrite ($Fe_2O_3 \cdot 0.5H_2O$) for the batch experiments. Bio-reduction of Fe(III)-(hydr)oxides can occur by two mechanisms (Pyzik and Sommer, 1981; Berner, 1984; Afonso and Stumm, 1992; Legall et al., 1994): directly by enzymatic catalysis and indirectly via chemical reaction with biogenic sulfide. As shown in Figure 2.7, the importance of both mechanisms was revealed by the accumulation of soluble Fe^{2+} during and after the consumption of lactate. Figure 2.7 also shows that the patterns of bacterial growth and substrate utilization with Fe(III) (hydr)oxides differed from the patterns with soluble iron. In contrast to the priority of

soluble Fe(III) utilization over sulfate utilization, the accumulation of soluble Fe^{2+} (attributed to solid-Fe(III) reduction) was observed only after all sulfate was reduced. This delayed reduction of Fe(III) from all Fe(III) (hydr)oxides is expected, as the crystalline phases of Fe(III) (hydr)oxides are less bioavailable than soluble Fe(III) due to the energetic need for extracellular electron transfer and dissolution of the Fe(III) solid (Lovley et al., 1993a; Weber et al., 2006). In addition, ferrihydrite was reduced more rapidly and completely than goethite and hematite, indicated by the higher concentration of accumulated soluble Fe^{2+}. This corresponds with ferrihydrite's larger surface area and higher redox potential. From any Fe(III) (hydr)oxide, the soluble Fe^{2+} concentrations were higher with pyruvate than with lactate, reflecting that using pyruvate as the electron donor led to more enzymatic reduction of Fe(III) (hydr)oxides by *D. vulgaris*.

The XRD patterns shown by Figure 2.8 reveal that mackinawite was present in the solid samples with ferrihydrite, although it was poorly crystallized. On the other hand, it is difficult to infer from the XRD data whether or not mackinawite was present from the bottles with goethite and hematite. Furthermore, a significant portion of hematite remained in the final solid samples. When pyruvate was the electron donor, the greater accumulation of soluble Fe^{2+} from hematite and ferrihydrite allowed precipitation of vivianite, along with the loss of soluble Fe^{2+} and phosphate.

The results of mass-balance modeling, shown in Figure 2.9, suggest that biogenic FeS solids produced from ferrihydrite were most abundant compared to goethite and ferrihydrite. Although it could not be detected by XRD, elemental S was present in the solid products from goethite and hematite according to the mass-balance calculation, suggesting that the enzymatic reduction dominated over chemical reduction of Fe(III).
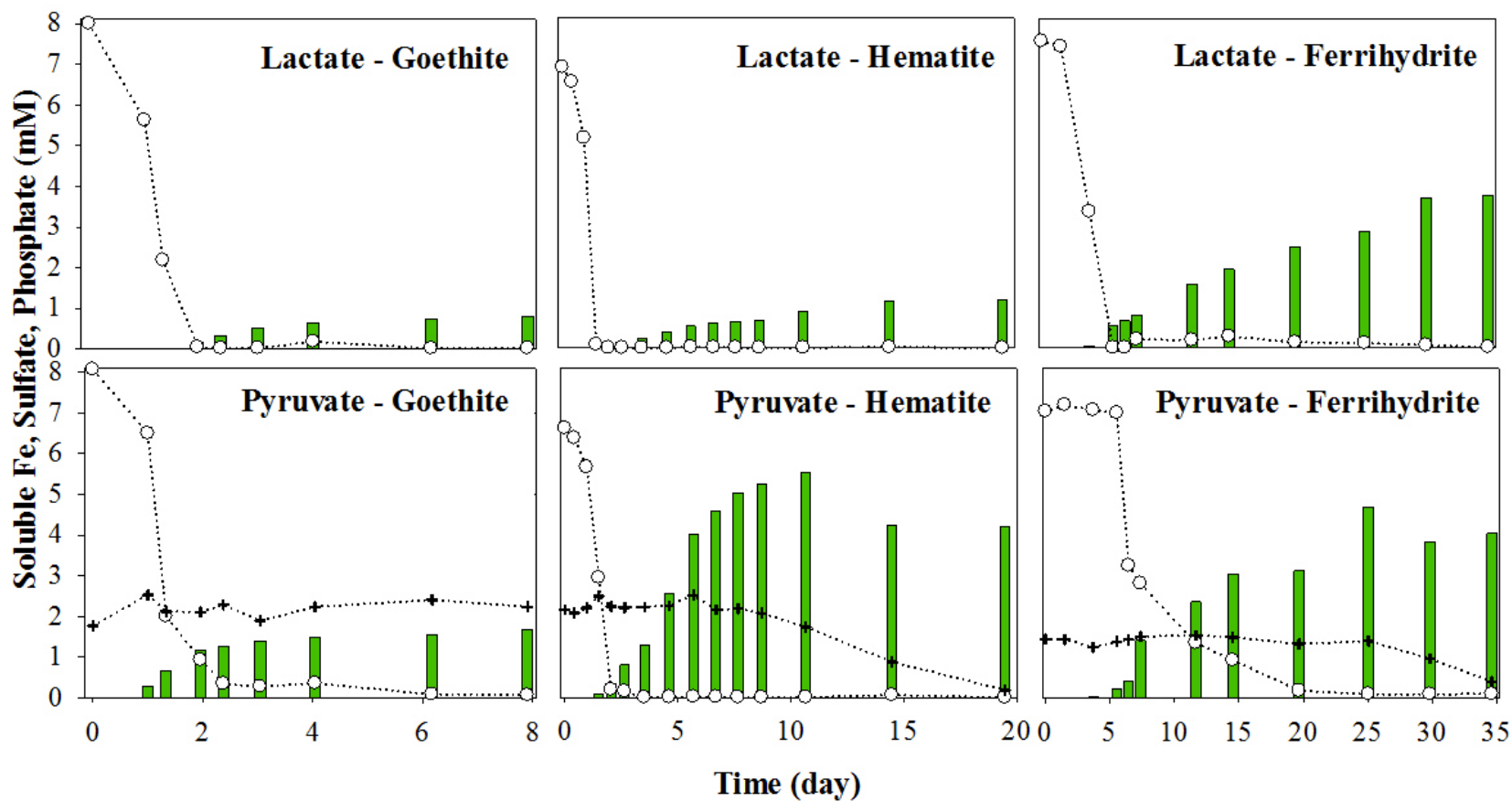
Figure 2.7. Concentrations of soluble Fe(II) (bars), sulfate (○), and phosphate (✚) during the growth of D. vulgaris with different electron donors and Fe(III) (hydr)oxides.

Figure 2.8. XRD spectra of synthetic goethite (maroon color), hematite (gold color), 2-line ferrihydrite (orange color), and solids separated from media (black color) with goethite as the iron source plus lactate as the electron donor (A), goethite + pyruvate (B), hematite + lactate (C), hematite + pyruvate (A), ferrihydrite + lactate (E), and ferrihydrite + pyruvate (F).

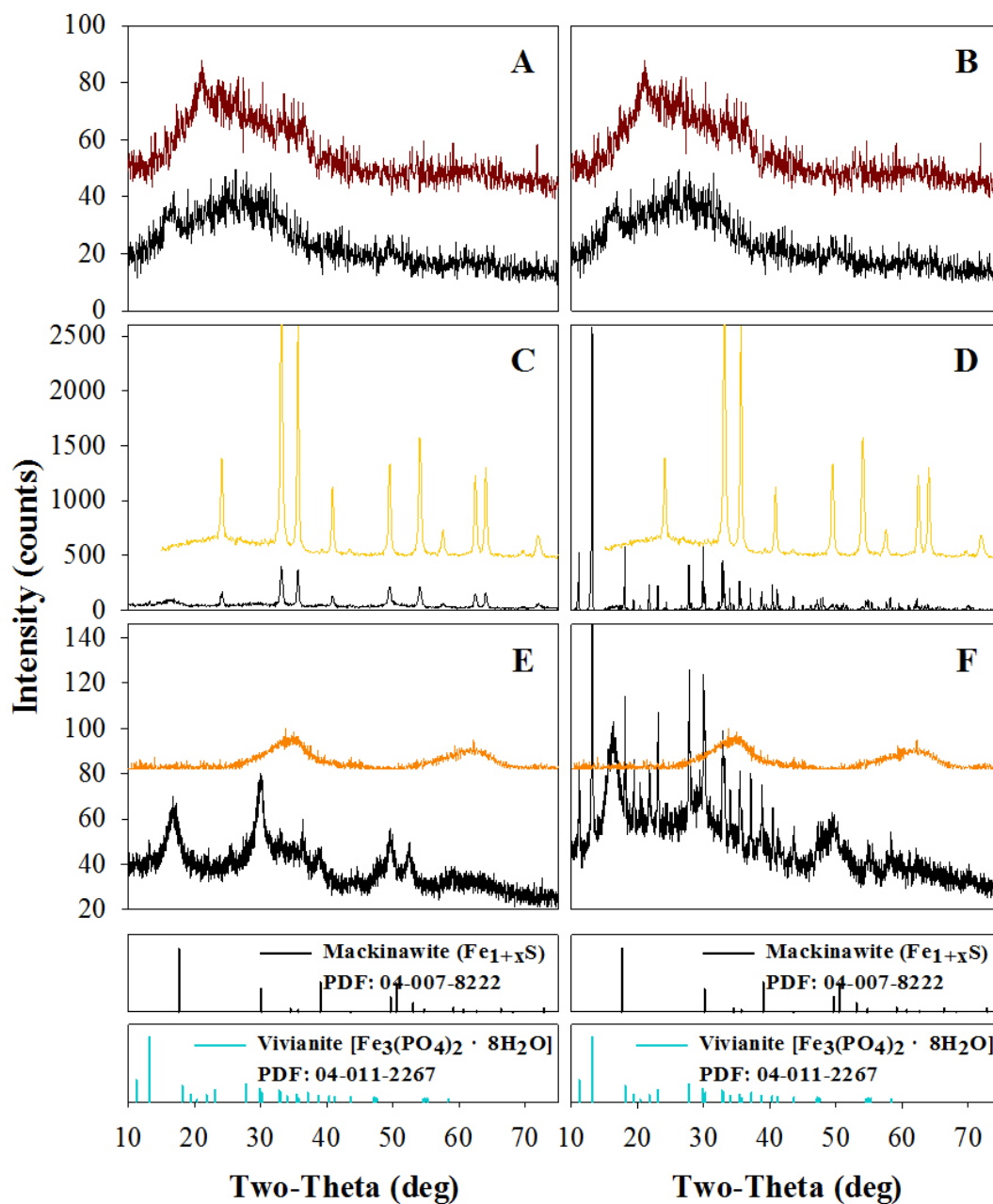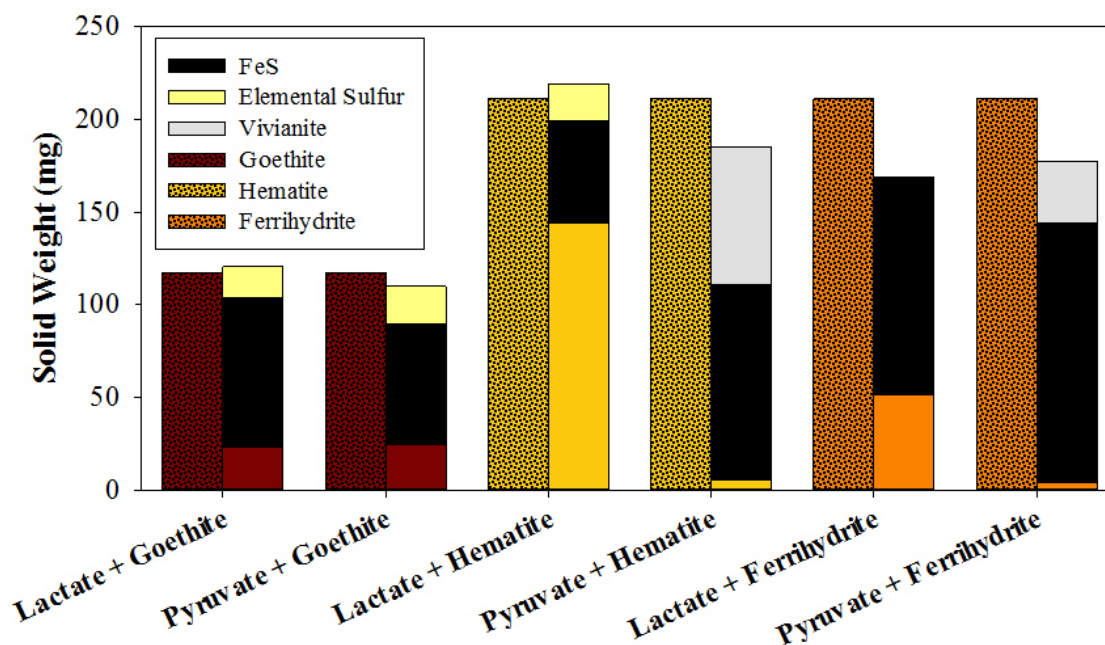**Figure 2.9**. The mass of Fe(III) hydroxide solids initially added to the 200 ml serum bottles (dotted bars) and the mass-balance-calculated final solid products (whole-colored bars).

In summary for this section, soluble Fe^{3+} reduction occurred preferentially over sulfate reduction due to its higher redox potential. However, Fe(III)-(hydr)oxide reductions were less favorable than sulfate reduction; in spite of sufficient electron donor, reductions of solid FE(III) was not complete. *D. vulgaris* produced mackinawite with either soluble Fe(II) or Fe(III) or with solid Fe(III) (hydr)oxide minerals. The mackinawite deriving from soluble Fe^{3+} was less crystallized than the mackinawite deriving from soluble Fe^{2+}, because retarded sulfate reduction delayed iron-sulfide formation. The mackinawite produced from Fe(III) (hydr)oxide solids was even less crystalline. Besides mackinawite, solids present at the end of the batch experiments included original Fe(III) (hydr)oxides, elemental sulfur, and vivianite [$Fe_3(PO_4)_2 \cdot 8(H_2O)$]. In terms of biogenic iron-sulfide production overall, soluble iron sources were able to be completely utilized, and thus were better than solid iron sources. In particular, soluble Fe^{2+} was better than soluble Fe^{3+} because it did not lower the pH, which accelerated mackinawite crystallization in our other experiments. Solid ferrihydrite led to less crystalline mackinawite, but was not completely utilized and led to other solid products alongside iron-sulfide. Thus, the solid iron hydroxides offer trade-offs when the practical goal is to produce more-amorphous biogenic iron-sulfide with higher activity for uranium sequestration.

2.3. U(VI) reduction by D. vulgaris

D. vulgaris is able to immobilize uranium by enzymatically reducing U(VI) to U(IV) (Lovley et al., 1993b; Barton et al., 1996), which precipitates as UO_2. We conducted batch experiments to evaluate enzymatic U(VI) reduction and UO_2 formation. Furthermore, the experiment investigated how the presence of SO_4^{2-} and/or Fe^{2+} affected the rate of U(VI) reduction and crystallization of biogenic UO_2.

We set up five anaerobic bottles with 1 mM uranyl (UO_2^{2+}) and with different experimental conditions involving the presence or absence of sulfate, soluble Fe^{2+}, and inoculum, as summarized in Table 2.1.

Table 2.1. The presence/absence of SO_4^{2-}, Fe^{2+}, and inoculum in the media of the five serum bottles

Bottle #	SO_4^{2-}	Fe^{2+}	Biomass suspensions
1	−	−	+
2	−	+	+
3	+	−	+
4	+	+	+
5 (control)	+	+	−

The results are summarized in Figure 2.10. U(VI) reduction occurred in the four inoculated bottles (left side of Figure 2.10). U(VI) reduction was fastest in Bottle 3 (with only SO_4^{2-}), in which 90% uranium reduction took about 20 hours. Sulfate reduction occurred in the two sulfate-containing bottles (3 and 4): 90% sulfate reduction occurred within 10 hours in Bottle 3 (with only SO_4^{2-}), while SO_4^{2-} reduction in Bottle 4 (with SO_4^{2-} and Fe^{2+}) was retarded during the first 48 hours, but reached 90% by 72 hours. The loss of soluble Fe^{2+} corresponded to sulfate loss and the formation of a distinct black color in Bottle 4 (with SO_4^{2-} and Fe^{2+}), indicating the formation of FeS. These results add weight to the observation by (Spear et al., 2000) that *D. desulfuricans* reduced uranium faster in the presence of sulfate, in contrast to U(VI) alone. We further interpret that free sulfide accelerated U(VI) reduction rate in Bottle 3, since abiotic reduction of U(VI) coupled with oxidation of dissolved sulfide to elemental sulfur (S^0) was shown in previous studies (Mohagheghi et al., 1985; Ho and Miller, 1986; Kosztolanyi et al., 1996).

The XRD patterns of solids separated from the four inoculated assay bottles are shown in the right side of Figure 2.10. Biogenic UO_2 was present in all four solid samples. The UO_2 in

Bottles 1 and 3 (no Fe^{2+}) was less crystalline than in Bottles 2 and 4 (with Fe^{2+}). This suggests that the presence of soluble Fe^{2+}, whether or not it was eventually precipitated, may have inhibited the crystallization process of biogenic UO_2. The inhibition probably was due to the selective interaction of soluble Fe^{2+} with a particular crystal face of growing crystal, which slowed the growth rate of the face relative to the other faces and alter the morphology of the crystal (Dang et al., 2007). Previous research (Dang et al., 2007; De Leeuw, 2002; Katz et al., 1993) reported that soluble Fe^{2+} inhibited the growth of crystals such as calcite and phosphoric acid hemihydrate, but its inhibitive effect on biogenic uraninite was never reported before.

XRD shows no clear signs of crystalline mackinawite in any of the bottles, although the formation of some iron-sulfide precipitate in Bottle 4 (with SO_4^{2-} and Fe^{2+}) was indicated by concomitant losses of SO_4^{2-} and soluble Fe^{2+}, as well as the very black color in the solution. Thus, formation of biogenic UO_2 might have inhibited the aging/crystallization of biogenic amorphous iron-sulfide. In addition, elemental sulfur (S^0) deriving from abiotic U(VI) reduction by sulfide was not shown in either XRD patterns, indicating that S^0 was probably amorphous.
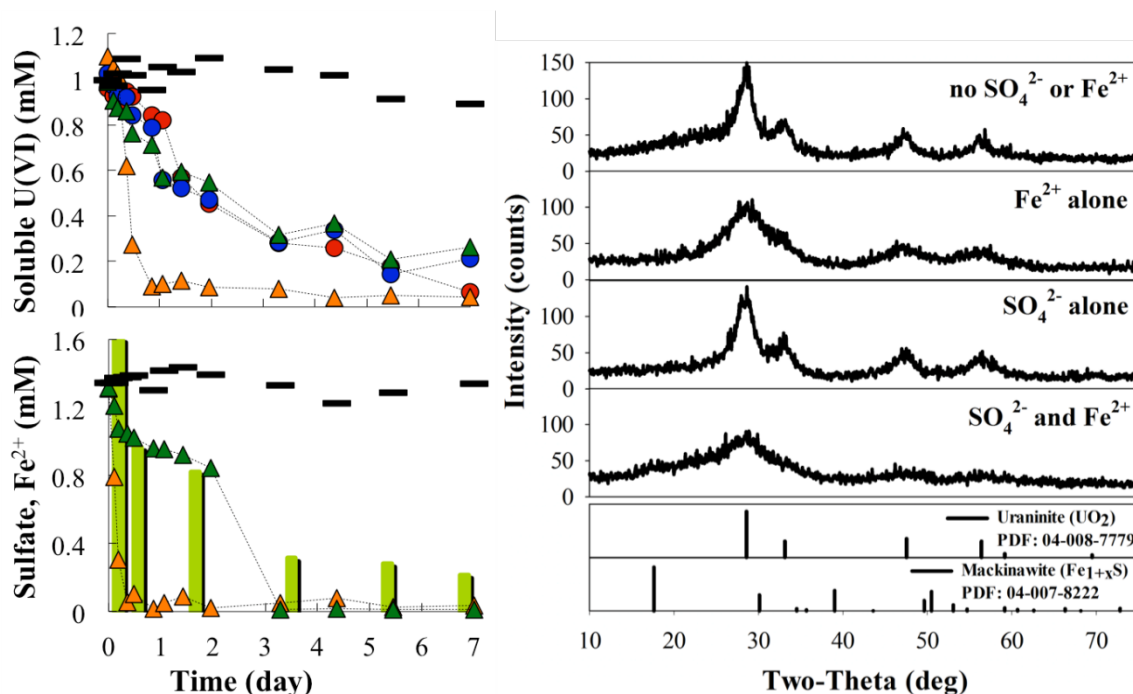
Figure 2.10. Concentrations of soluble U(VI) and sulfate from assay bottles 1 (no SO_4^{2-} or Fe^{2+}, ●), 2 (Fe^{2+} alone, ●), 3 (SO_4^{2-} alone, ▲), 4 (both SO_4^{2-} and Fe^{2+}, ▲), and 5 (control, -); and concentration of ferrous (bars) from Bottle 4 (left); XRD spectra of solids from Bottle 1 (no SO_4^{2-} or Fe^{2+}), Bottle 2 (Fe^{2+} alone), Bottle3 (SO_4^{2-} alone), and Bottle 4 (SO_4^{2-} and Fe^{2+}) (bottom).

In summary for this section, our experiments with U(VI) demonstrated that *D. vulgaris* enzymatically reduced soluble U(VI) to crystalline UO_2. U(VI) reduction was fastest when proceeding in parallel with sulfate reduction and in the absence of soluble Fe^{2+}, as sulfide also was a potent U(VI) reductant acting in parallel with enzymatic reduction of U(VI). In terms of solids characteristics, the presence of iron seemed to inhibit crystallization of biogenic UO_2, while the formation of biogenic UO_2 may in turn have inhibited the crystallization/aging of biogenic iron-sulfide. In terms of U bioremediation, these results imply that biogenic UO_2 may be less crystalline than the synthetic UO_2 and thus more subject to being re-oxidized.

2.4 References

Abdelouas, A., Lutze, W., and Nuttall, H. E., 1999. Oxidative dissolution of uraninite precipitated on Navajo sandstone. *Journal of Contaminant Hydrology* **36**, 353-375.

Afonso, M. D. and Stumm, W., 1992. Reductive Dissolution of Iron(III) (Hydr)oxides by Hydrogen-Sulfide. *Langmuir* **8**, 1671-1675.

Barton, L. L., Choudhury, K., Thomson, B. M., Steenhoudt, K., and Groffman, A. R., 1996. Bacterial reduction of soluble uranium: The first step of in situ immobilization of uranium. *Radioact Waste Manag* **20**, 141-151.

Berner, R. A., 1984. Sedimentary Pyrite Formation: An Update. *Geochim Cosmochim Ac* **48**, 605-615.

Heidelberg, J. F., Seshadri, R., Haveman, S. A., Hemme, C. L., Paulsen, I. T., Kolonay, J. F., Eisen, J. A., Ward, N., Methe, B., Brinkac, L. M., Daugherty, S. C., Deboy, R. T., Dodson, R. J., Durkin, A. S., Madupu, R., Nelson, W. C., Sullivan, S. A., Fouts, D., Haft, D. H., Selengut, J., Peterson, J. D., Davidsen, T. M., Zafar, N., Zhou, L. W., Radune, D., Dimitrov, G., Hance, M., Tran, K., Khouri, H., Gill, J., Utterback, T. R., Feldblyum, T. V., Wall, J. D., Voordouw, G., and Fraser, C. M., 2004. The genome sequence of the anaerobic, sulfate-reducing bacterium Desulfovibrio vulgaris Hildenborough. *Nat Biotechnol* **22**, 554-559.

Herbert, R. B., Benner, S. G., Pratt, A. R., and Blowes, D. W., 1998. Surface chemistry and morphology of poorly crystalline iron sulfides precipitated in media containing sulfate-reducing bacteria. *Chemical Geology* **144**, 87-97.

Ho, C. H. and Miller, N. H., 1986. Formation of Uranium Oxide Sols in Bicarbonate Solutions. *J Colloid Interf Sci* **113**, 232-240.

Kosztolanyi, K., NGuyen, T. C., LHote, F., and Vernet, M., 1996. Reduction of uranyl complexes and precipitation of uranium oxides by means of hydrogen sulphide gas. *Magy Kem Foly* **102**, 180-187.

Legall, J., Payne, W. J., Chen, L., Liu, M. Y., and Xavier, A. V., 1994. Localization and Specificity of Cytochromes and Other Electron-Transfer Proteins from Sulfate-Reducing Bacteria. *Biochimie* **76**, 655-665.

Li, Y. L., Vali, H., Yang, J., Phelps, T. J., and Zhang, C. L., 2006. Reduction of Iron Oxides Enhanced by a Sulfate-Reducing Bacterium and Biogenic H2S. *Geomicrobiol J* **23**, 103-117.

Lovley, D. R., Giovannoni, S. J., White, D. C., Champine, J. E., Phillips, E. J. P., Gorby, Y. A., and Goodwin, S., 1993a. Geobacter-Metallireducens Gen-Nov Sp-Nov, a Microorganism Capable of Coupling the Complete Oxidation of Organic-Compounds to the Reduction of Iron and Other Metals. *Arch Microbiol* **159**, 336-344.

Lovley, D. R., Widman, P. K., Woodward, J. C., and Phillips, E. J. P., 1993b. Reduction of Uranium by Cytochrome c3 of Desulfovibrio vulgaris. *Appl Environ Microb* **59**, 3572-3576.

Mohagheghi, A., Updegraff, D. M., and Goldhaber, M. B., 1985. The Role of Sulfate-Reducing Bacteria in the Deposition of Sedimentary Uranium Ores. *Geomicrobiol J* **4**, 153-173.

Moon, H. S., Komlos, J., and Jaffé, P. R., 2009. Biogenic U(IV) oxidation by dissolved oxygen and nitrate in sediment after prolonged U(VI)/Fe(III)/SO42- reduction. *Journal of Contaminant Hydrology* **105**, 18-27.

Pyzik, A. J. and Sommer, S. E., 1981. Sedimentary Iron Monosulfides - Kinetics and Mechanism of Formation. *Geochim Cosmochim Ac* **45**, 687-698.

Sani, R. K., Peyton, B. M., Amonette, J. E., and Geesey, G. G., 2004. Reduction of uranium(VI) under sulfate-reducing conditions in the presence of Fe(III)-(hydr)oxides. *Geochimica Et Cosmochimica Acta* **68**, 2639-2648.

Spear, J. R., Figueroa, L. A., and Honeyman, B. D., 2000. Modeling reduction of uranium U(VI) under variable sulfate concentrations by sulfate-reducing bacteria. *Appl Environ Microb* **66**, 3711-3721.

Voordouw, G., 2002. Carbon monoxide cycling by Desulfovibrio vulgaris Hildenborough. *J Bacteriol* **184**, 5903-5911.

Weber, K. A., Achenbach, L. A., and Coates, J. D., 2006. Microorganisms pumping iron: anaerobic microbial iron oxidation and reduction. *Nat Rev Microbiol* **4**, 752-764.

Wilkin, R. T. and Barnes, H. L., 1996. Pyrite formation by reactions of iron monosulfides with dissolved inorganic and organic sulfur species. *Geochimica Et Cosmochimica Acta* **60**, 4167-4179.

Wilkin, R. T. and Barnes, H. L., 1997. Formation processes of framboidal pyrite. *Geochim Cosmochim Ac* **61**, 323-339.

3. Abiotic reduction of U(VI) by FeS and sulfide

In this study we examined U(VI) reactions with the either ferrous monosulfide mineral mackinawite or aqueous sulfide, both potentially important reductants of U(VI) in uranium contaminate groundwater. U(VI) reactions with mackinawite or sulfide are potentially important in assessing U sequestration mechanisms by geochemical or biogeochemical processes under sulfate reducing conditions.

For the mackinawite study, the objective was to determine the mechanisms of U(VI) sorption reactions with mackinawite under variable pH, using batch uptake data, extractions by carbonate solution, equilibrium modeling, and X-ray absorption spectroscopy. Specifically, the study aimed to test the hypothesis that iron(II) sulfide mackinawite only partially reduces U(VI), with both reduction to U(IV) phases and U(VI) adsorption responsible for U removal from a simple electrolyte solution in a CO_2 and O_2 free system.

In the aqueous sulfide study, U(VI) reactions with aqueous sulfide were studied under a range of geochemical conditions including pH, carbonate, and Ca concentrations. X-ray absorption spectroscopy (XAS) was used for characterizing solid phases formed by the U(VI) reaction with aqueous sulfide under different geochemical conditions. The research questions of this study were to assess: 1) the U(VI) reaction products produced; and 2) the most important geochemical solution variables controlling abiotic U(VI) reduction by aqueous sulfide.

3.1 Study of U(VI) reduction by FeS

Previous experimental studies reported partial reduction of U(VI) by a variety of iron(II) sulfide minerals, including amorphous iron sulfide, mackinawite, and pyrite.[7-9] In this study we examined U(VI) reactions with the ferrous monosulfide mineral mackinawite. Understanding U reactions with mackinawite is important in assessing U sequestration mechanisms by geochemical or biogeochemical processes under sulfate reducing conditions. The objective of this study was to investigate the mechanisms of U(VI) sorption reactions with mackinawite under variable pH using batch uptake data, extractions by carbonate solution, equilibrium modeling, and X-ray absorption spectroscopy (XAS). Specifically, the study aimed to test the hypothesis that iron(II) sulfide mackinawite only partially reduces U(VI), with both reduction to U(IV) phases and simple adsorption of U(VI) responsible for U removal from a simple electrolyte solution in a CO_2 and O_2 free system.

U(VI) uptake by mackinawite as a function of pH is shown in Figure 3.1, along with the U(VI) aqueous speciation as a function of pH. At the initial uranium concentration of 5×10^{-5} M, uranium removal was complete over the entire experimental pH range between 5 and 11. U-reacted mackinawite samples were extracted using an anoxic 14.4 mM bicarbonate and 2.8 mM carbonate mixed solution (CARB) at pH 9.4. The extraction result showed that less than 10% of the U associated with mackinawite was extracted, regardless of the sorption pH (Figure 3.1). The result shows that CARB-extractable, reversibly and loosely bound U(VI) is a minor U species, whereas the non-extractable, irreversibly bound U phase is a major U species in the U(VI) reaction with mackinawite. The possible irreversibly bound U species may include a U(IV) solid phase, a mackinawite surface bound molecular U(IV) species, and U(VI) species incorporated into the structure of mackinawite or its oxidation products.

Transmission electron microscopic results of U reacted with mackinawite at a higher initial U concentration of 1.4×10^{-4} M and lower mackinawite loading of 1 mM are given in Figure 3.2. This sample was prepared by reacting dissolved U(VI) with sulfide solution and then adding ferrous solution to precipitate mackinawite. For this higher U concentration and much lower Fe/U ratio condition, TEM was successfully used to study the microstructural characteristics of U association with mackinawite. Figure 3.2A is a conventional bright-field (BF) image showing U distribution on the mackinawite aggregates. The smaller, dark spots are U-rich parts and the bigger, lighter parts are mackinawite. The micrograph shows that U rich particles are rather evenly distributed over the mackinawite particles. Figure 3.2B is a high angle annular dark-field (HAADF) image taken from the same area as imaged in the Figure 3.2A (rotated by 90 degrees) showing U association with mackinawite. In the HAADF image, the brighter areas are U rich and the darker areas are the lighter elemented mackinawite. Once again, the micrograph confirms the even distribution of U-rich particles over mackinawite particles. Figure 3.2C is a selected area electron diffraction (SAED) pattern of the U-rich particles. The pattern is interpreted to be an isometric unit cell with a dimension of 5.46 Å, consistent with uraninite (UO_{2+x}). High resolution lattice fringe imaging showed close microtextural relations between the resulting uraninite and elemental S suggesting elemental S as the oxidation product under the experimental condition (Figure 3.2D).
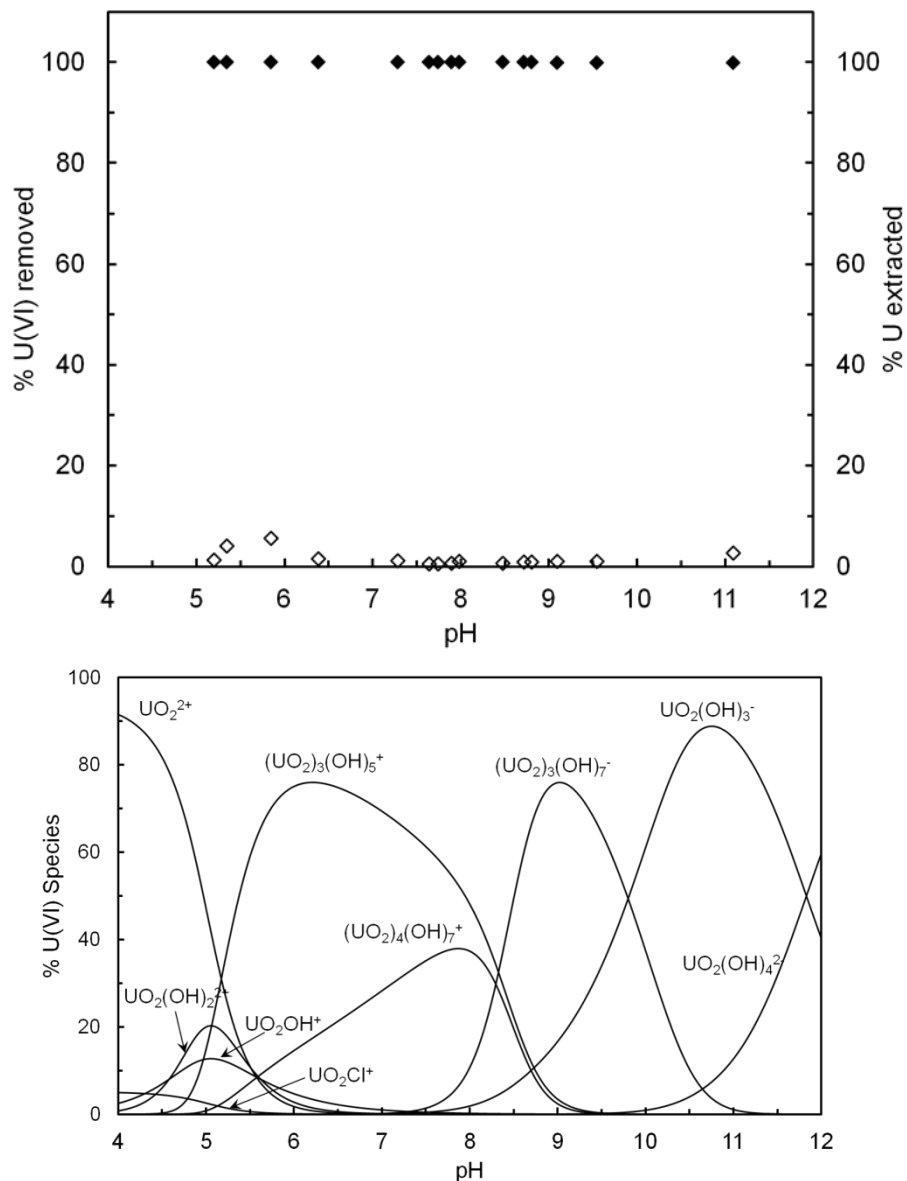
Figure 3.1. The amounts of U(VI) removed by macknawite (filled diamond) as a function of solution pH in the reaction of 5×10^{-5} M U(VI) reacted with a 5g/L mackinawite suspension in 0.1 M NaCl electrolyte solution under an O_2 and CO_2 free atmosphere and the corresponding amounts of U extracted by CARB solution at pH 9.4 (open diamond) from the U-reacted mackinawite under the various pH condition. Lower panel is the initial U(VI) aqueous speciation under the experimental condition as a function of pH. U(VI) removal from solution is almost complete over the whole pH range tested, independent of the U(VI) aqueous speciation.
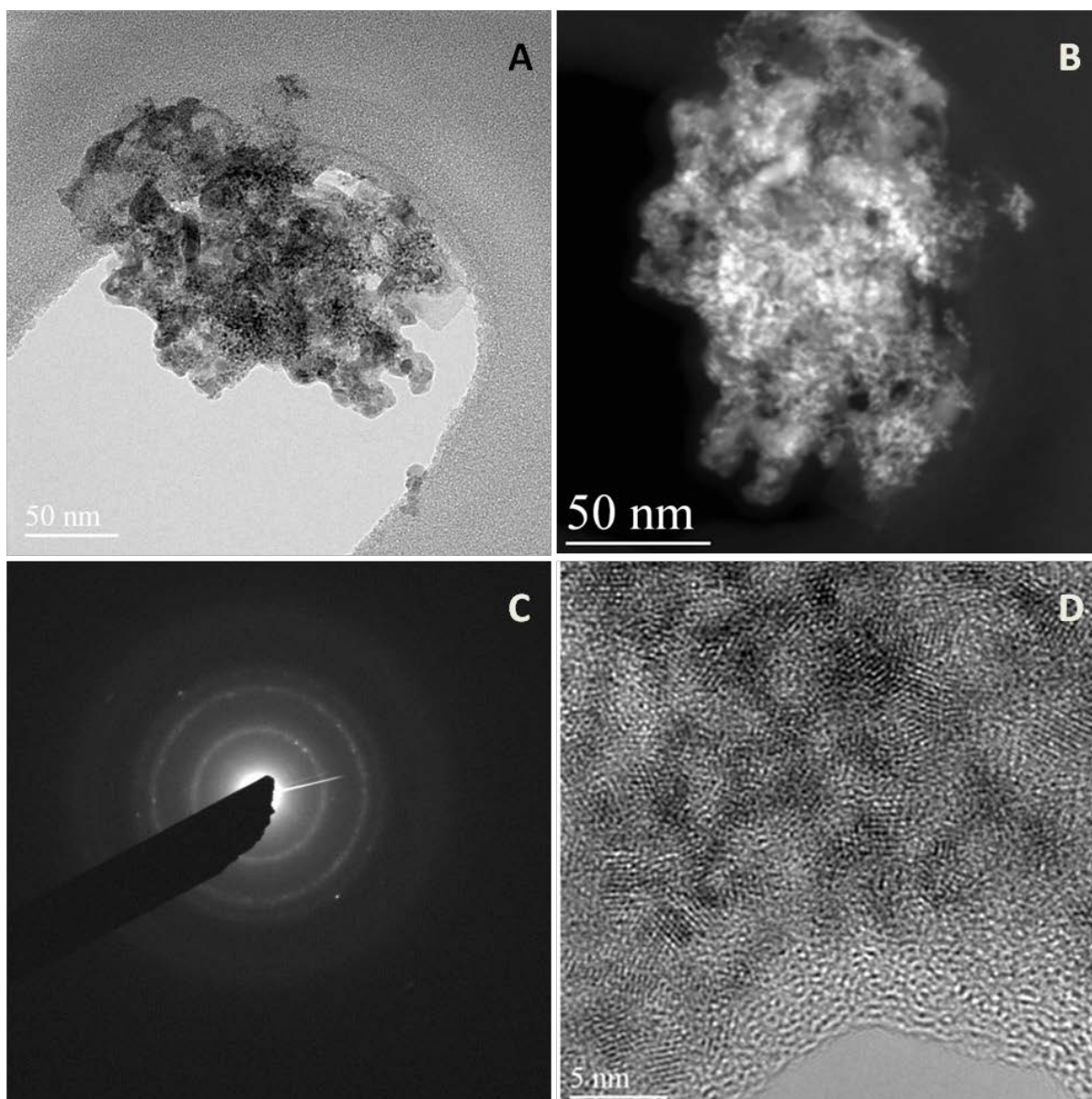
Figure 3.2. TEM results of U(VI) reacted with mackinawite at 140 uM U and 1 mM mackinawite and pH 7.3. A) BF image of uraninite nanoparticles (smaller, dark particles) associated with mackinawite particles (larger, brighter particles) . B) HAADF image showing uraninite (bright spots) association with mackianwite (dark spots). C) SAED pattern confirming the U(VI) phase was nanocrystalline uraninite. D) HREM lattice image directly showing the nanocrystalline nature of uraninite closely associated with elemental S.

This study suggests that U(VI) reduction by the iron sulfide mineral mackinawite may be an important process occurring under certain ambient field conditions, such as at the Old Rifle site. U(VI) interaction with mackinawite is a possible process leading to the U association with pyrite framboids observed at the Rifle site. The resistance of uraninite against oxidation in the presence

of sufficient mackinawite also supports the retention of U in the solid phase during oxidative transformation of mackinawite to pyrite. Therefore, the U association with mackinawite reported in this study suggests a plausible mechanism for initial U association with nanoscale mackinawite particles leading to an eventual U association with framboidal pyrite, as found at the Rifle site.

3.2 Study of U(VI) reduction by Sulfide

Upon reaction of U(VI) with aqueous sulfide, one set of literature has reported the formation of a partially reduced mixed-valent U solid phase (Moyes et al., 2000; Wersin et al., 1994; Livens et al., 2004). However, in other studies, such as Hua and Deng (2008) and Hua et al. (2006), the formation of $UO_{2(s)}$ (i.e., uraninite) has been reported from the U(VI) reaction with ferrous sulfide or aqueous sulfide in Ca-free systems and with organic buffers to control pH. To explore the basis for these different endpoints, the present work used more realistic conditions by including dissolved Ca and rather than organic buffers pH was controlled through changing the carbonate concentration. For this study, the reduction of U(VI) by sulfide was investigated over a range of pH, U(VI), S(-II), carbonate (CARB), and Ca concentration. Their effects are described in turn below.

Solution pH. When the reaction pH was 10.8, dissolved U concentration did not decrease as a function of reaction time (not shown). However, when the pH was titrated down to 7, dissolved U concentration immediately decreased to below detection within less than an hour. This observation shows that U reduction by aqueous sulfide is favorable under circumneutral pH conditions, while it is not favorable under basic pH conditions. The typical pH range of the Rifle groundwater is between 6.62 and 7.42 with the mean value of 6.94, suggesting that abiotic U reduction by aqueous sulfide may be a feasible U reduction mechanism at the site if other conditions are favorable. The results in the Ca and CARB amended systems suggest that solution pH not only affects the rate of U(VI) reduction by aqueous S(-II), but also determines the identity of the solid phase reaction product.

Dissolved S(-II). Dissolved U concentration as a function of time is presented in Fig. 3.3 in the reaction of U(VI) with different aqueous sulfide concentrations. Other conditions were 0.19 mM initial U(VI) and 1 mM carbonate without added Ca. The U removal rate increased with

increasing dissolved sulfide concentration. When the dissolved sulfide concentration was 10 mM, the dissolved U concentration immediately decreased to below detection within half an
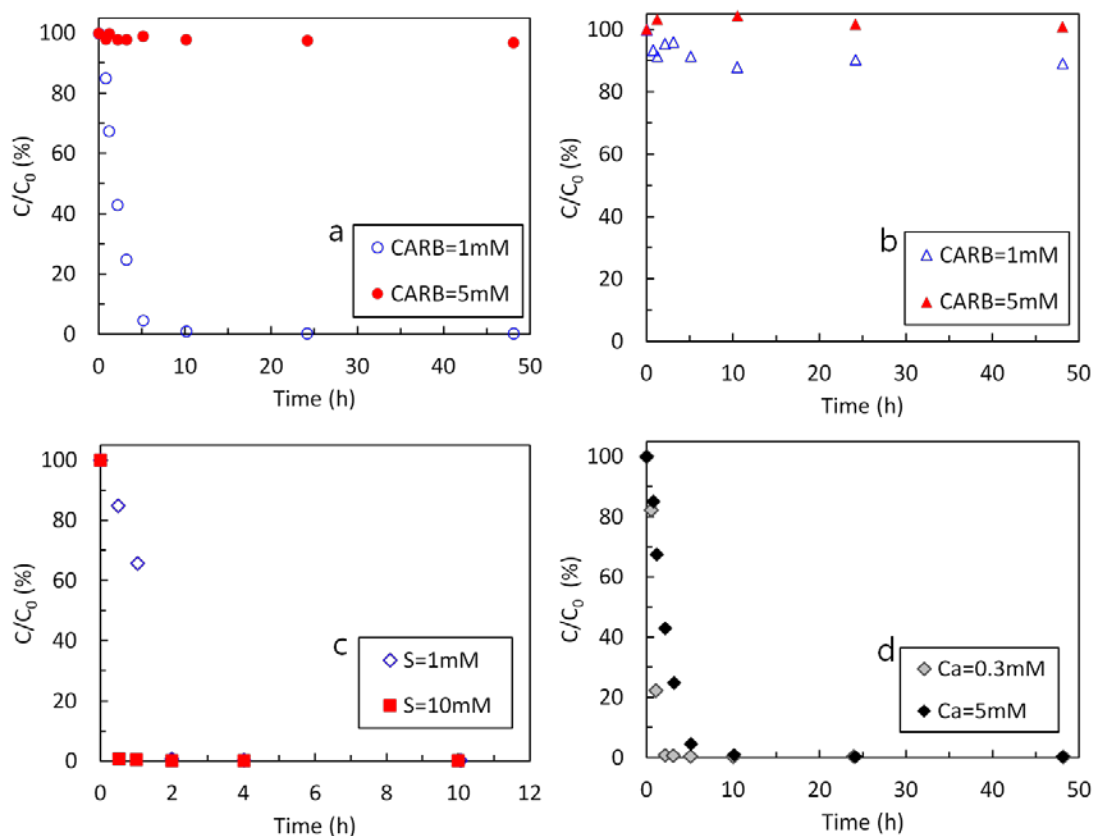

Figure 3.3. Effects of geochemical variables on the U(VI) reduction by aqueous sulfide: (a) initial U(VI) = 5.5×10^{-5} M, pH 7, Ca = 5mM, HS$^-$ = 1mM, (b) initial U(VI) = 3.5×10^{-7} M, pH 7, Ca = 5 mM, HS$^-$=1 mM, (c) initial U(VI) = 1.9×10^{-4} M, pH 7, total carbonate = 1 mM, no Ca added, and (d) initial U(VI) = 5×10^{-5} M, pH 7, total carbonate = 1mM, HS$^-$ = 1 mM)

hour. The dissolved U concentration had a dropped off less dramatically to reach below detection after ~2 h of reaction when reacted with 1 mM S(-II).

U(VI) concentration. When the initial U(VI) was 5.5×10^{-5}M, U reduction was clearly observed in the reaction with 1mM dissolved sulfide under 1mM carbonate and 5mM Ca concentration condition (Fig. 3.3a). When the initial U(VI) concentration was lowered to 3.5×10^{-7} M, U reduction was much slower under the same experimental conditions with 1 mM carbonate concentrations (Fig. 3.3b). Under 5mM dissolved carbonate concentration, U removal rate was much slower for both initial U concentrations (Fig. 3.3a and 3.3b).

Calcium concentration. Increased Ca concentration slowed the U(VI) removal rate (Fig. 3.3c). When the dissolved Ca concentration was 0.3mM, dissolved U reached below detection within 2h from the start of the reaction, whereas it took 10h to reach below detection when Ca concentration was 5mM. Other conditions were S 1mM, carbonate 1mM, and U of 5×10^{-5}M.

Carbonate concentration. The carbonate effect observed in Fig. 3.3 in conjunction with U concentration was further studied in more detail (Fig. 3.4). Initial carbonate concentration was varied between 1 and 5 mM. Other conditions were 4×10^{-5} M U(VI), 5 mM Ca^{2+}, 1mM HS^-, and pH 7. Rapid decrease in dissolve U concentration occurred under the 1 mM carbonate condition (Fig. 3.4). U removal rate was slowed as the dissolved carbonate concentration increased to 1.5, 2.0, and 3.0 mM. No reduction was observed when the carbonate concentration was raised to 5.0 mM (Fig. 3.4). This is an important observation considering that 5.0 mM and higher carbonate concentrations are not uncommon within the Rifle aquifer.
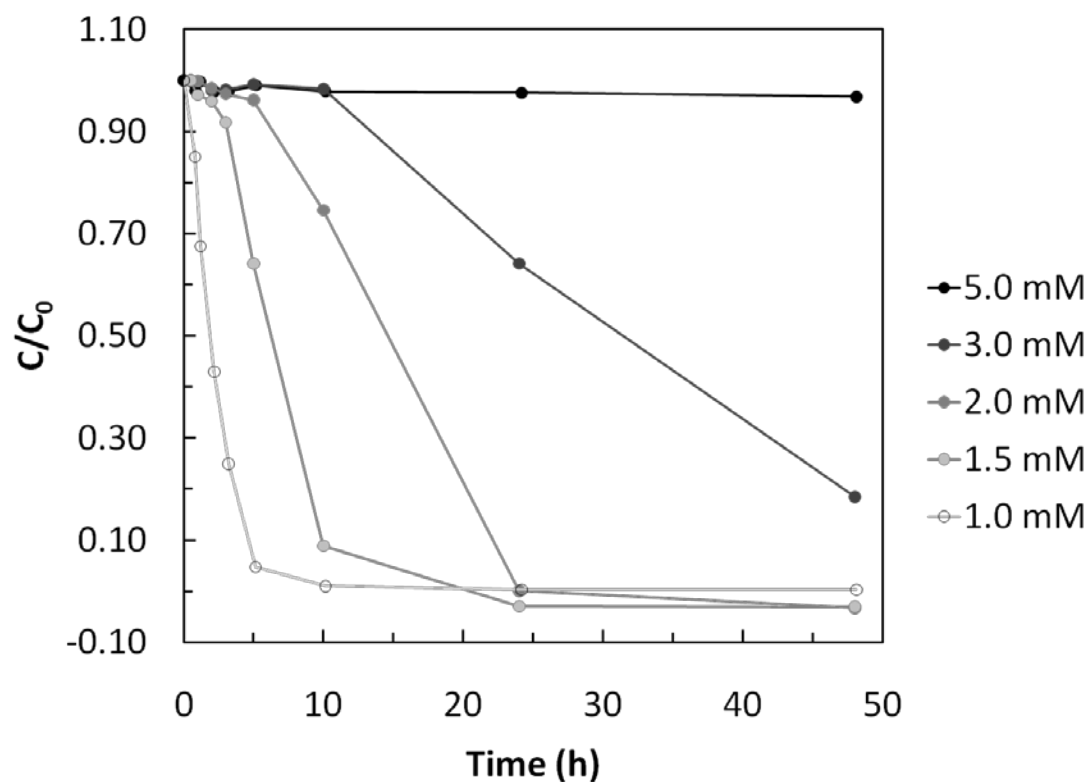

Figure 3.4. Changes in dissolved U(VI) concentration as a function of time in the reaction of U(VI) with HS- under different dissolved carbonate concentration conditions: U(VI) = 4x10-5M, Ca = 5mM, HS-= 1mM, and pH = 7).

The solid phase reaction products in the reaction of U(VI) with aqueous sulfide were characterized using XRD, TEM, and XAS. The XRD, TEM, and XAS results of the dark precipitate observed at pH 7 in the Ca- and CARB-free system are given in Figure 3.5. Both XRD and selected area electron diffraction confirmed that the precipitate formed by the homogeneous reaction of aqueous U(VI) and aqueous sulfide was uraninite under circumneutral pH in this simple model system with only dissolved U(VI), sulfide, nitrate, sodium, H$^+$, and OH$^-$ in anoxic water. XAS gives an independent set of information as to the solid phase U speciation. XANES shows that the edge position of the U L_{III}-edge X-ray absorption spectrum shifted to 17171 eV, ca. 2 eV lower than the starting U(VI) solution. This indicates U reduction to U(IV).
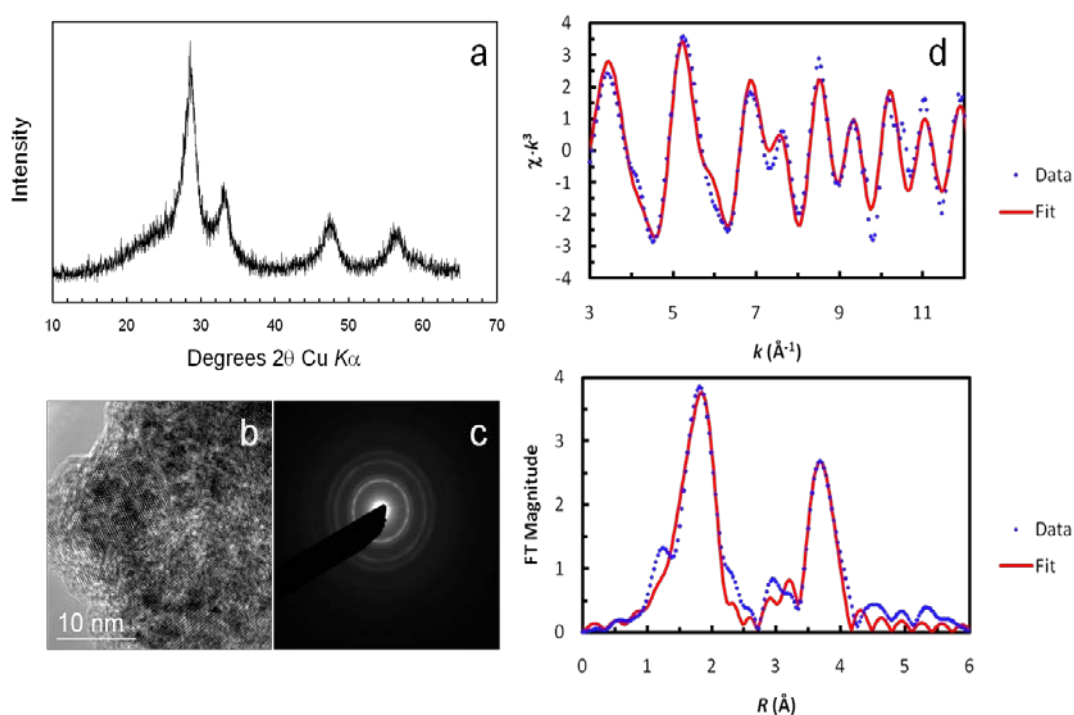

Figure 3.5. The U(VI) reaction product with aqueous sulfide formed at pH 7 in the Ca- and CARB-free model system. (a) The dark precipitate's X-ray diffraction pattern, (b) high resolution lattice fringe image, (c) selected area electron diffraction pattern, and (d) X-ray absorption spectroscopy results. The precipitate is uraninite.

EXAFS analysis gives structural parameters of 6.5 nearest oxygen neighbors at the interatomic distance of 2.32 Å from the central U atom and of 2.5 second shell uranium neighbors at 3.84 Å (Table 1). These structural parameters are consistent with the reported

structure of uraninite, although the coordination number for the uranium shell is lower than that expected for a well crystalline uraninite. Similar observation of low coordination number for the nearest U atoms is reported to be due to the nanocrystalline nature of the uraninite precipitate in a study of uraninite formation from U(VI) reaction with green rust or mackinawite. The characterization of the solid phase reaction product confirms that in the system without Ca or CARB, U(VI) is reduced to nanoscale uraninite under the circumneutral pH by reaction with aqueous sulfide, but U(VI) remains as dissolved U(VI) without formation of any solid phase under the basic pH condition. The following 1:1 stoichiometric relation between U(VI) and S(-II) was suggested for the U(VI) reduction by dissolved sulfide under similar experimental conditions:[5]

$$UO_2^{2+} + HS^- \rightarrow UO_{2(s)} + S^0_{(s)} + H^+ \hspace{3cm} \text{Equation 3.1}$$

The 1st derivative XANES spectra of the solid phases precipitated in the Ca and CARB added systems under circumneutral pH conditions, namely 6.7, 7.1, and 7.3 are given in Figure 3.6a. The solid samples have the maximum 1st derivative points moved to a lower energy (17171 eV), compared with 17173 eV of the starting U(VI) solution. The energy position of the samples is similar to that of the synthetic uraninite. The circumneutral pH samples also have minimum 1st derivative positions similar to that of synthetic uraninite. The 2nd derivative XANES spectra show that the pH 6.7, 7.1, and 7.3 sample line up well with the uraninite model. This observation indicates that the dark precipitate formed from the homogeneous reaction of aqueous U(VI) and S(-II) in the presence of Ca and CARB under circumneutral pH conditions is a U(IV) solid. The EXAFS parts of the XAS spectra were reduced and analyzed (Figure 3.6b and Table 1). All the solid samples precipitated under circumneutral pH conditions, ranging from 6.7 to 7.3, have structural parameters similar to those of synthetic uraninite model compound (Table 1). The first atomic shell has a single oxygen shell instead of the starting U(VI) solution's distinct double shell composed of equatorial and axial oxygen atoms characteristic of uranyl ion.
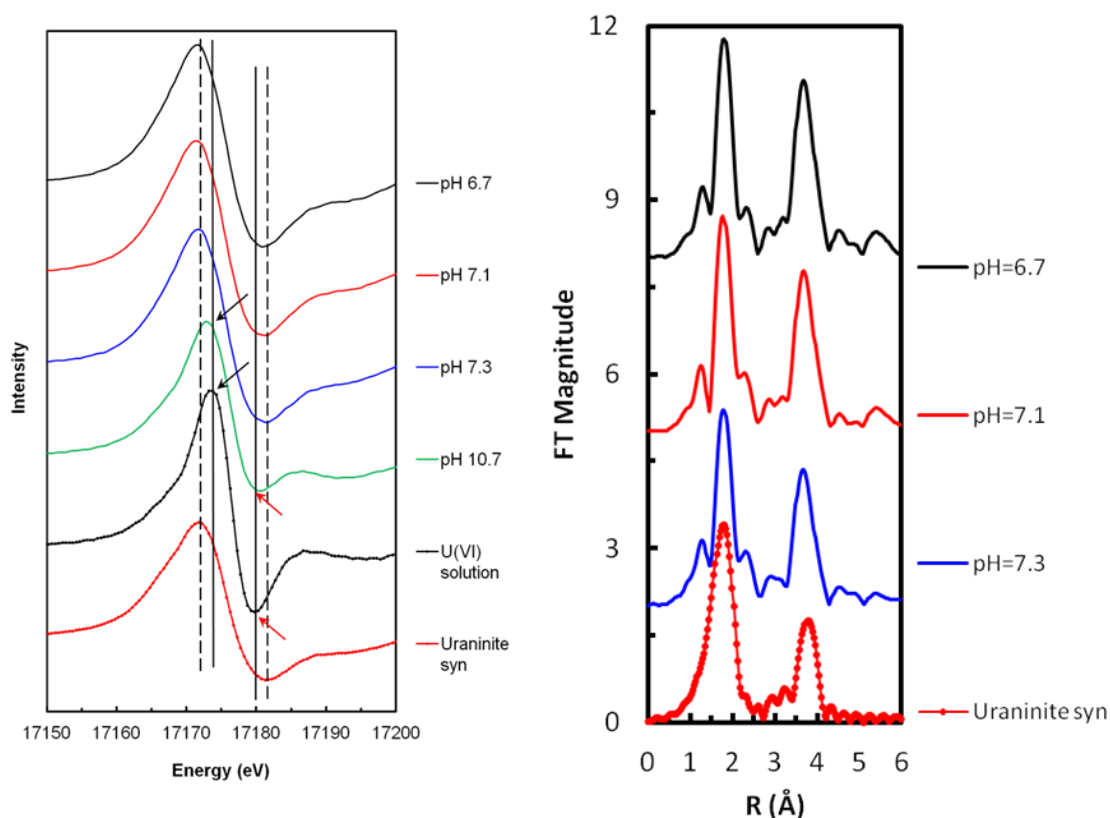
Figure 3.6. (a) 1st derivative U L_{III} edge XANES spectra of U reaction products along with those of the U(VI) solution and synthetic uraninite model compounds; (b) EXAFS of U(VI) reacted with dissolved sulfide (CARB = 1mM, Ca = 5mM, S = 1mM, and U = 0.1mM).

The interatomic distances of first shell oxygen atoms ranged from 2.32 to 2.33 Å. These values are in good agreement with the reported ranges for synthetic, biogenic, and hydrothermal uraninite specimens (Schofield et al., 2008; Sharp et al. 2009; Singer et al. 2009; Wyckoff, 1978). The distinct second shell feature at 3.85 Å originating from the strong backscattering by U neighbors excludes possibilities of molecular U(IV) monomers recently reported for U(VI) reduction by microorganisms with P-containing ligand presence. These EXAFS structural parameters suggest precipitation of uraninite in the homogeneous reaction of U(VI) with aqueous sulfide under circumneutral pH in the presence of Ca and CARB.

Table 1. Structural parameters extracted from the EXAFS analysis (N: coordination number of backscatterer atoms around the absorber U atom, R: interatomic distance in Å unit of the absorber-backscatterer pair, σ^2 : Debye-Waller factor of the absorber-backscatterer pair'.

Shell		pH 7.3	pH 7.1	pH 6.7	Uaq 1000 ppm	Uraninite Feff 8.10 calculated	Uraninite Synthetic
O	N	5.8	6.5	6.1		8	6.5
	R	2.32	2.33	2.32		2.3678	2.25
	σ^2	0.0105	0.0109	0.0098		0	0.0164
U^{IV}	N	5.3	5.4	5.3		12	2.5
	R	3.81	3.81	3.81		3.8666	3.84
	σ^2	0.0079	0.0069	0.0062		0	0.0071
O_{ax}	N				2.4		
	R				1.77		
	σ^2				0.0030		
O_{eq}	N				4.8		
	R				2.42		
	σ^2				0.0061		

This study demonstrates that U(VI) can be reduced to U(IV) by reaction with aqueous sulfide under certain combinations of experimental conditions relevant to the Rifle aquifer. In general, higher sulfide, higher U(VI), lower pH, lower dissolved carbonate, and lower Ca concentrations provided favorable conditions for abiotic U reduction by aqueous sulfide under the experimental conditions studied. At circumneutral pH relevant to the Rifle aquifer, the products of electron transfer reaction between aqueous sulfide (major species HS⁻) and U(VI) were elemental sulfur and nano-scale uraninite as evidenced by X-ray diffraction, X-ray absorption spectroscopy, and transmission electron microscopy. This is consistent with the results by Hua et al. (2006), although they used different experimental conditions, including the use of pH buffer, higher carbonate concentration, and the absence of Ca.

3.3 References

Moyes, L.N.; Parkman, R.H.; Charnock, J.M.; Vaughan, D.J.; Livens, F.R.; Hughes, C.R.; Braithwaite, A. Uranium uptake from aqueous solution by interaction with goethite, lepidocrocite, muscovite, and mackinawite: An X-ray absorption spectroscopy study. *Environ. Sci. Technol.* **2000**, *34*, 1062-1068.

Wersin, P.; Hochella, Jr., M.F.; Persson, P.; Redden, G.; Leckie, J.O.; Harris, D.W. Interaction between aqueous uranium(VI) and sulfide minerals: Spectroscopic evidence for sorption and reduction. *Geochim. Cosmochim. Acta* **1994**, *58*, 2829-2843

Livens, F. R.; Jones, M. J.; Hynes, A. J.; Charnock, J. M.; Mosselmans, J. F. W.; Hennig, C.; Steele, H.; Collison, D.; Vaughan, D. J.; Pattrick, R. A. D.; Reed, W. A.; Moyes, L. N. X-ray absorption spectroscopy studies of reactions of technetium, uranium, and neptunium with mackinawite. *J. Environ. Radioactiv*. **2004**, *74*, 211-219

Hua, B.; Deng, B. Reductive immobilization of uranium(VI) by amorphous iron sulfide. *Environ. Sci. Technol.* **2008**, *42*, 8703-8708.

Hua, B.; Xu, H.; Terry, J.; Deng, B. Kinetics of uranium(VI) reduction by hydrogen sulfide in anoxic aqueous systems. *Enviorn. Sci. Technol.* **2006**, *40*, 4666-4671

Schofield, E.J.; Veeramani, H.; Sharp, J.O.; Suvorova, E.; Bernier-Latmani, R.; Mehta, A.; Stahlman, J.; Webb, S.M.; Clark, D.L.; Conradson, S.D.; Ilton, E.S.; Bargar, J.R. Structure of biogenic uraninite produced by Shewanella oneidensis strain MR-1. *Environ. Sci. Technol.* **2008**, 42, 7898-7904.

Sharp, J.O.; Schofield, E.J.; Veeramani, H.; Suvorova, E.I.; Kennedy, D.W.; Marshall, M.J.; Mehta, A.; Bargar, J.R.; Bernier-Latmani, R. Structural similarities between biogenic uraninites produced by phylogenetically and metabolically diverse bacteria. *Environ. Sci. Technol.* **2009**, 43, 8295-8301.

Singer, D.M.; Farges, F.; Brown, Jr., G.E. Biogenic nanoparticulate UO_2: Synthesis, characterization, and factors affecting surface reactivity. *Geochim. Cosmochim. Acta* **2009**, 73, 3593-3611.

Wyckoff, R.W. G. *Crystal Structures.* John Wiley & Sons, New York, 1978.

4. Investigating the mechanisms of iron sulfide in inhibiting UO$_2$ reoxidation

Long-term stability of reduced U(IV) solids may be achieved when dissolution and/or reoxidation of UO$_2$ are sufficiently slow during occasional or low levels of oxidant intrusion. In U-contaminated aquifers, iron sulfides, when naturally occurring, may provide an additional reservoir of reducing capacity for U immobilization (Bargar et al., 2013). However, relatively few studies have investigated the reactions of UO$_2$ with FeS or the protective nature of FeS in inhibiting UO$_2$ oxidation.

The UM team carried out batch and flow-through reactor studies to understand the mechanisms and kinetics of the oxidative dissolution of reduced U(IV) solids in the presence of iron sulfide under simulated groundwater conditions. Batch studies examined the mechanism of the oxidation reaction of UO$_2$(s) by dissolved oxygen in the presence and absence of synthetic FeS(s). Continuously mixed flow-through reactors (CMFRs) were utilized for examining the inhibition kinetics of UO$_2$ oxidation by FeS under oxic groundwater conditions under various geochemical conditions.

In the following sections, we present our results in three sections that correspond to journal manuscripts that have been published or submitted for publication. They address (1) the role of FeS as an effective oxygen scavenger to inhibit the dissolution of UO$_2$; (2) the impact of geochemical conditions, i.e., pH, FeS content, and DO concentrations, on the inhibited oxidative dissolution rate of UO$_2$ in the presence of FeS; and (3) the potential of FeS oxidation products as oxidants for UO$_2$ mobilization after FeS consumption by oxygen. In each section, we highlight the most important results by presenting a condensed version of the journal manuscript.

4.1 Reoxidation Processes of UO$_2$ in the Presence of FeS

In the first study, the oxidative transformation of UO$_2$ nanoparticles by oxygen was investigated in the presence of FeS under simulated groundwater conditions. In this study, a batch reactor was equipped with a water jacket for temperature control and a multi-port lid for accommodating various probes, sampling, and gas mixtures with fixed partial pressures of P_{O2} = 0.02 atm, and P_{CO2} = 0.05 atm. Oxidation products and U speciation were monitored as a function of time in a strictly abiotic system. The kinetic profiles of dissolved U in Figure 4.1 show that FeS inhibited UO$_2$ dissolution for about 51 hr by effectively scavenging oxygen and keeping DO levels low. After FeS was depleted due to its oxidation, the DO level increased, and

UO_2 oxidative dissolution occurred at an initial rate of $r_m = 1.2 \pm 0.4 \times 10^{-8}$ mol·g^{-1}·s^{-1}, higher than $r_m = 5.4 \pm 0.3 \times 10^{-9}$ mol·g^{-1}·s^{-1} in the control experiment where FeS was absent.
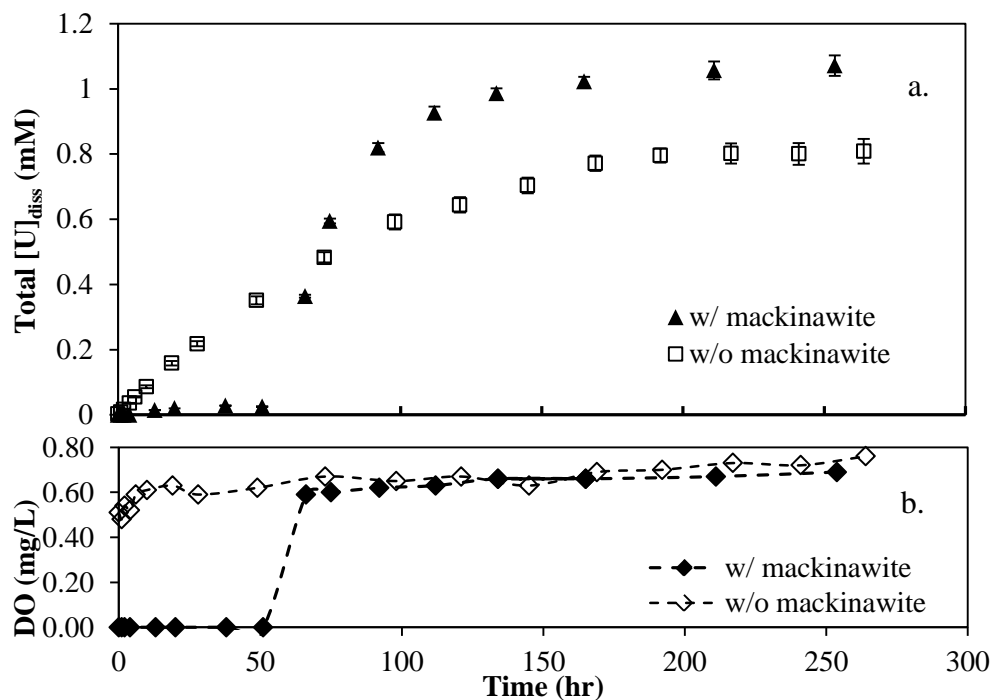

Figure 4.1. Comparison of kinetic profiles of (a) total dissolved U and (b) DO in the presence (*filled markers*) and absence (*empty markers*) of FeS over the course of the oxidation experiment. Error bars reflect one analytical standard deviation of analysis and are sometimes smaller than the symbol size.

As a result of FeS rapidly consuming oxygen, solid-phase U remained as U(IV) until FeS was nearly completely oxidized, as shown by the Fourrier transforms in Figure 4.2. Meanwhile, the oxidation of FeS resulted in the formation of predominantly Fe(III) oxyhydroxides and elemental sulfur. Following the complete oxidation of FeS, oxidative dissolution of UO_2 began. The subsequent adsorption of multinuclear U(VI)-carbonato complexes by nanogoethite or lepidocrocite was a major retention mechanism for the dissolved U(VI) species formed during UO_2 oxidation, and no evidence was seen for U(VI) incorporation into the Fe(III) mineral structure (Fig.1). The presence of Fe(III) oxyhydroxide solids seemed to accelerate UO_2 oxidative dissolution compared to the control by facilitating the electron transfer from U(IV) to oxygen.

These results confirm that the stability of reduced U(IV) solid phases was achieved in the presence of FeS nanoparticles as a result of the rapid and preferential scavenging of DO by FeS. Thus, FeS-associated U(IV), which has been observed following active bioreductive *in situ*

treatment of U(VI) contaminated groundwater, may be protected against oxidative dissolution for sustained periods under fluctuating redox conditions in subsurface.
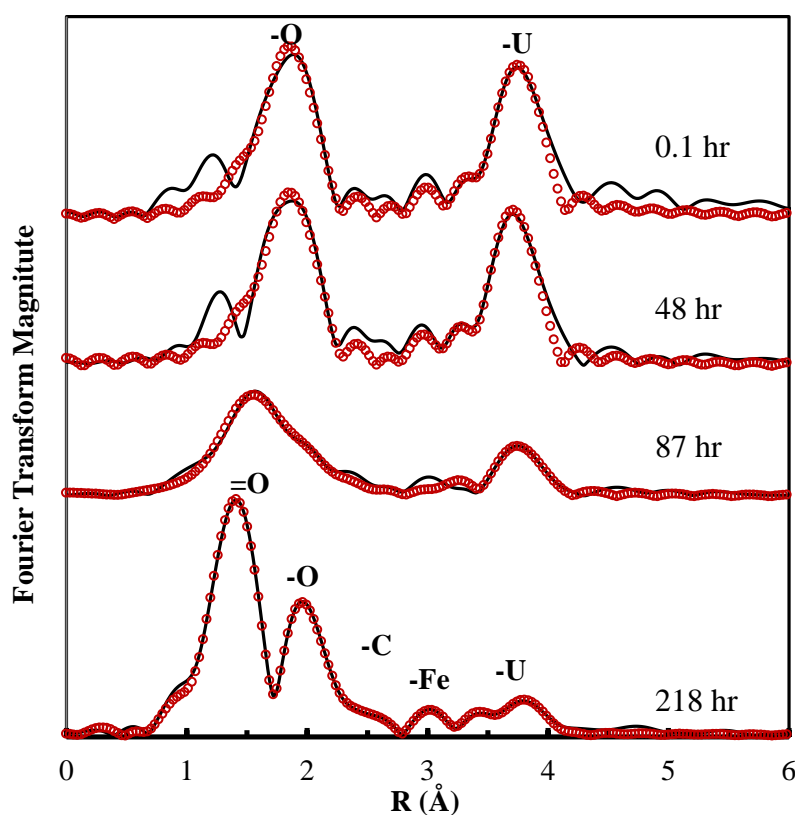

Figure 4.2. Fourier transform magnitudes of U L_{III}-edge EXAFS in the samples over the course of oxidative dissolution experiment in the presence of FeS (black line: data, red dots: fits).

While FeS scavenges DO and keeps DO levels low, it undergoes significant oxidation to produce Fe(III) oxyhydroxide solids and elemental sulfur, as evidenced by the X-ray diffraction patterns in Figure 4.3. Ferrihydrite was the intermediate Fe(III) product, and it quickly transformed to more stable nanogoethite and lepidocrocite after 120 hr reaction with oxygen. In comparison, S_8^0 was the primary S oxidation product throughout the experiment, with little thiosulfate ($S_2O_3^{2-}$) or sulfate (SO_4^{2-}) detected from the aqueous solution. These results confirm that elemental sulfur was the major intermediate products of structural S(-II) of FeS in an abiotic system.
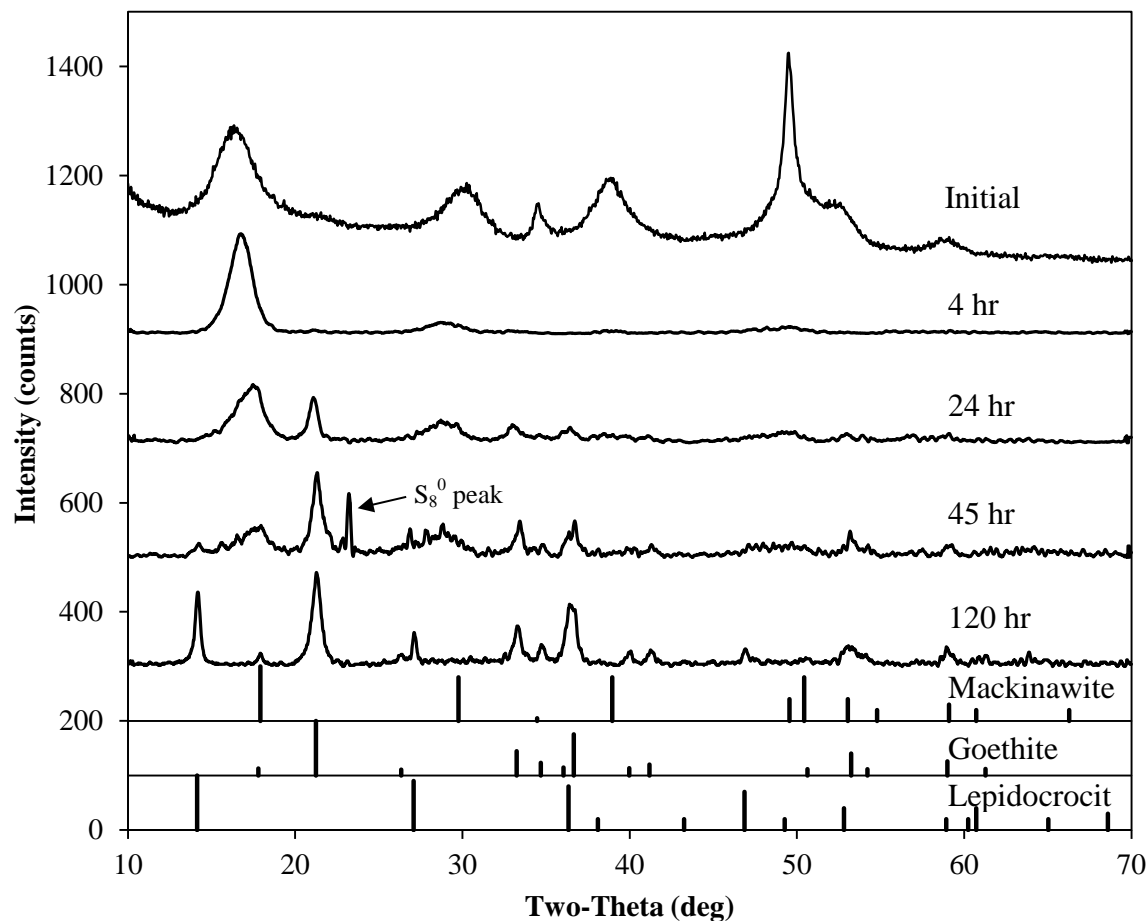
Figure 4.3. Diffraction patterns of oxidized samples in the batch system. Oxidation times are indicated inside the diffractograms.

4.2 Dissolution Rate of UO₂ during FeS-Inhibited Reoxidation by Oxygen

Flow-through reactor experiments in this study examined the kinetics of U(IV) oxidative dissolution in the presence of nanoparticulate FeS with oxygen supplied as the oxidant at varied pH, DO concentrations, and FeS values. The results are summarized in Figure 4.4. In the presence of FeS, the oxidative dissolution of UO_2 was inhibited and resulted in low U concentration (<1 μM) over the range of solution conditions. For the three pH conditions studied, FeS reduced the rate of UO_2 dissolution by more than an order of magnitude compared to the rates in its absence (Figure 4.4a). FeS inhibited UO_2 oxidative dissolution by consuming the DO entering into the CSTR. With an influent DO concentration of 1.8 mg·L^{-1}, FeS reduced the DO level in the CSTR to <0.5 mg·L^{-1} as measured in the effluent solution by a DO probe, which has a detection limit of ~0.2 mg·L^{-1}. Higher DO levels -- between 1.3–1.9 mg·L^{-1} -- were

observed in effluent for control experiments in absence of FeS, consistent with the influent DO levels. With similar levels of DO, the UO_2 dissolution rates were independent of pH in this study. At pH 7.1 and FeS concentration of 18.7 mM, the inhibited UO_2 dissolution rate increased with increasing DO concentration (Figure 4.4b), but remained significantly lower than the control with no FeS. In comparison, at a fixed UO_2 concentration of 0.48 mM, pH = 7, and DO = 1.8 mg·L^{-1}, higher FeS concentration resulted in lower $[U]_{ss}$ and UO_2 dissolution rate (Figure 4.4c).
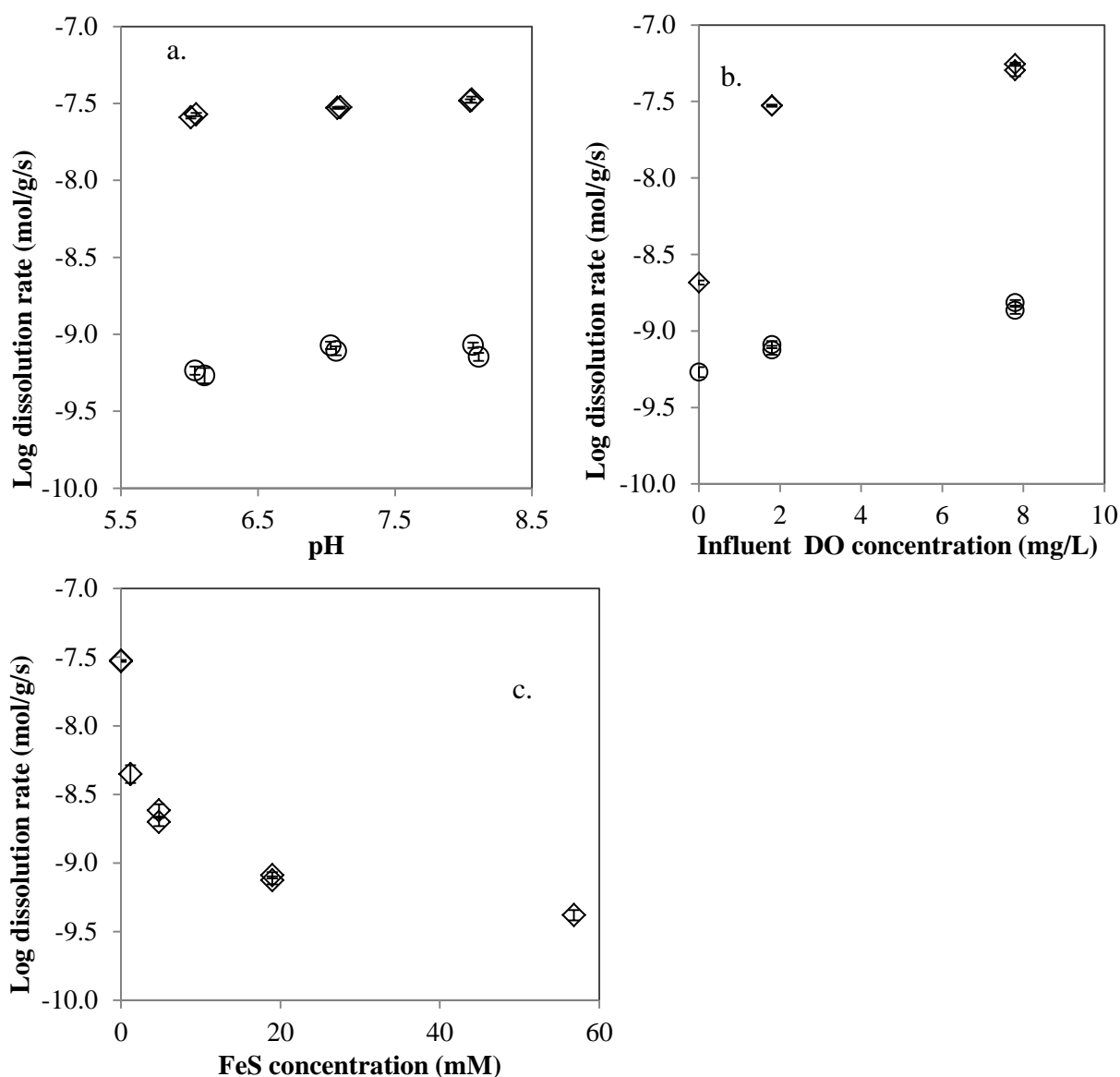

Figure 4.4. Steady-state UO_2 dissolution rates (mol·g^{-1}·s^{-1}) determined in the presence (○) and absence (◊) of FeS as a function of (a) pH; (b) DO concentration (mg·L^{-1}) at 18.7 mM FeS and pH 7.1; and (c) FeS concentration (g/L) at pH 7.1. Error bars represent 95% confidence interval of 6 to 10 individual measurements of dissolution rates.

The consumption of DO by FeS was accompanied by a pH-dependent Fe(II) release into the effluent solution. At pH 6.1, considerable FeS dissolution resulted in greater dissolved Fe(II) concentration compared to higher pH (Figure 3). The pH-dependent release of dissolved Fe(II) in oxic groundwater resulted in a loss of reducing capacity of FeS, which consequently decreased the duration of the FeS inhibition of UO_2 particle oxidation. The aqueous Fe(II) species only slowly oxidized under pH < 6.5 (Morgan and Lahav, 2007) and contributed little to overall scavenging of oxygen in the reactor. At basic pH, structural Fe(II) of FeS was oxidized directly to produce solid phase Fe(III) products. The complete solid-phase conversion of Fe(II) to Fe(III) -- with little Fe(II) dissolution -- utilized nearly the entire reducing capacity of FeS and thus extended the inhibition period of UO_2 dissolution.
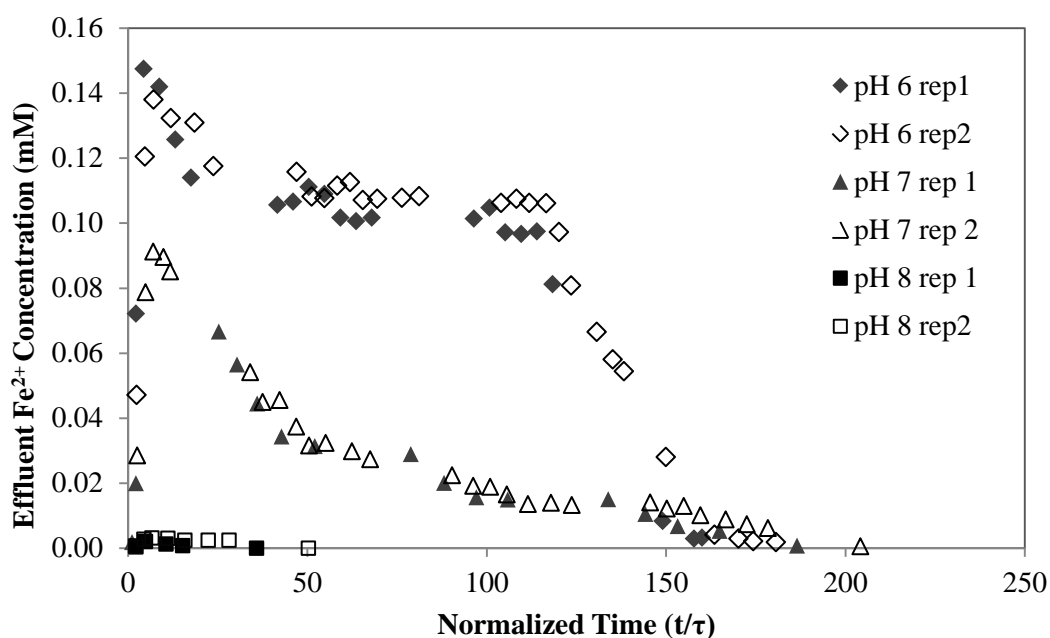

Figure 4.5. The dissolved Fe^{2+} release profiles from FeS dissolution at different pH in artificial groundwater containing 1.8 mg/L DO. Replicates are represented in filled or empty markers.

FeS dictates DO levels in the simulated groundwater solution, and its concentration therefore influences the UO_2 oxidative dissolution mechanism and the corresponding rate-limiting process. At relatively high FeS concentrations (18.7 mM), no evidence for a U(VI) surface coating on reacted UO_2 samples was found from XAS analyses, suggesting the step of UO_2 surface oxidation determined the overall dissolution rate. The detachment of surface complexes (Ca-UO_2-CO_3^{2-} complexes) occurred faster relative to surface oxidation, preventing U(VI) from accumulation. In contrast, a partially oxidized UO_2 was revealed by XANES spectrum in the

control reactor when exposed to relatively high influent DO in the absence of FeS. The detachment of surface-bound U(VI) into solution may become rate limiting, although facilitated by carbonate and calcium ions. Similarly, Ulrich et al. (2009) determined the detachment of U(VI)-carbonato complexes as rate-limiting in the presence of carbonate, since oxidation of surface U(VI) is fast under mildly oxidizing conditions (DO = ~0.6 mg·L^{-1}). By using a strong oxygen scavenger such as FeS, however, the rate-limiting step of UO_2 dissolution can be shifted.
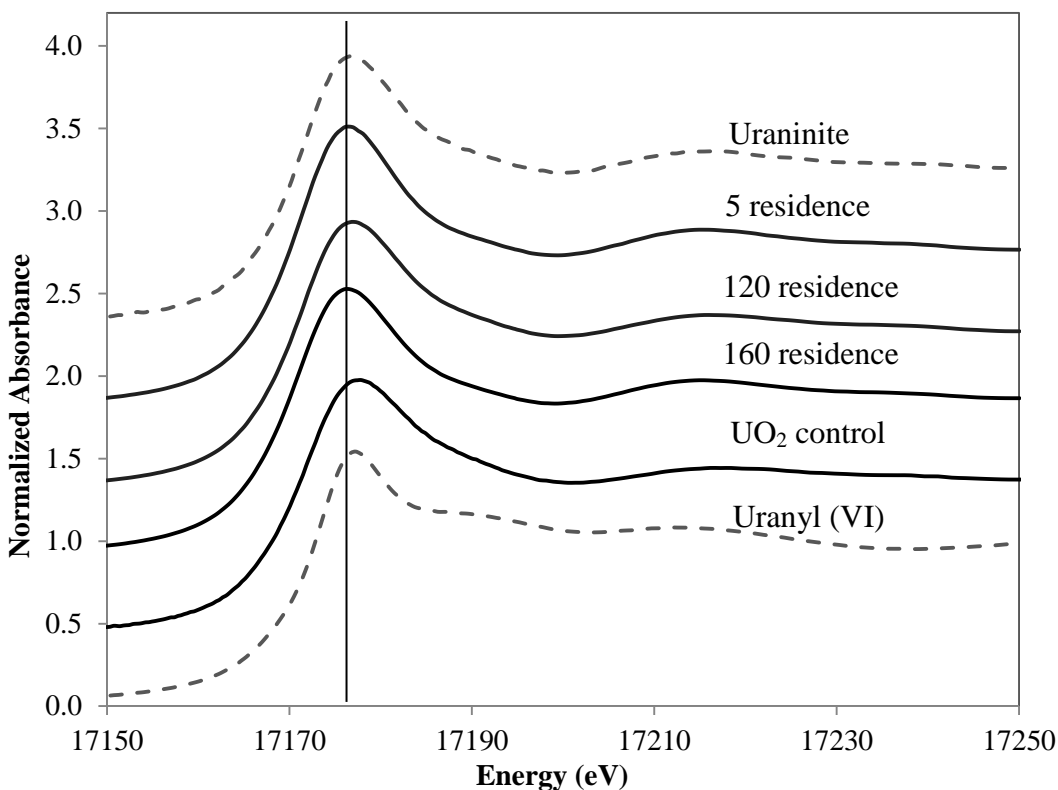

Figure 4.6. Uranium L_{III}-edge XANES spectra of batch samples as a function of time in the presence of FeS. The dotted lines bracket in the peak position of U(IV) in uraninite. An energy shift to higher eV indicates oxidation of U to higher valence state.

In summary for this section, the surface-oxidation step controlled the overall UO_2 dissolution rate in the presence of synthetic nano-FeS when effective oxygen scavenging by FeS lowered the DO to rate-limiting levels. Because nanocrystalline FeS is readily formed under sulfate reducing conditions (Abdelouas et al., 1999b; Rickard and Morse, 2005), FeS may provide practical protection of UO_2 in the field when oxic conditions are not prevalent.

4.3 Enhanced release of U(VI) from FeS post-oxidation products.

As previously discussed, the preferential oxidation of FeS by oxidants may lead to the production of Fe(III) oxides and elemental sulfur. The exhaustion of FeS after biostimulation can result in exposure of reduced U(IV) solids to the oxidants, which are capable of remobilizing uranium. Sani et al. (2005) and Ginder-Vogel et al. (2006) showed that iron oxides can accelerate abiotic oxidative dissolution of reduced U solids, but the relationship between the type and amount of Fe(III) on the rate of U reoxidation has not been fully examined.

Flow-through reactor was employed to investigate the dissolution pattern of UO_2 after FeS was consumed by oxygen in the groundwater solution. The results are presented in Figure 4.7. After a phase of inhibited dissolution of UO_2 during oxygen scavenging by FeS, oxygen breakthrough occurred in the CSTR as a result of FeS depletion. The dissolved U concentration started to increase immediately in response to the higher DO levels found in the reactor. Unlike control experiments, UO_2 dissolution showed a sharp increase of released U concentration without reaching a steady state. The dissolved U quickly diminished after the peak and dropped continuously to small values. Figure 4.7 shows that higher FeS concentration resulted in longer inhibition duration but higher peak $[U]_{diss}$ after FeS was completely oxidized.
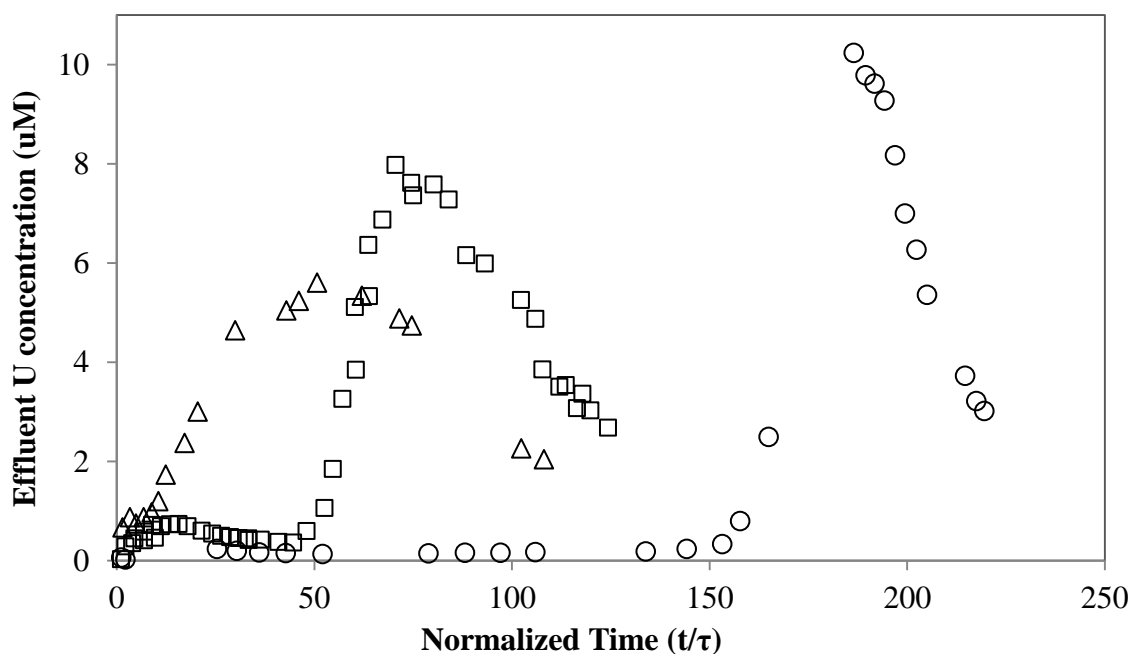

Figure 4.7. The total dissolved U release profiles in the presence of different FeS concentrations (○) 18.7 mM (□) 4.8 mM and (◊) 1.2 mM under pH =7 and 1.8 mg/L DO artificial groundwater solution.

The fast release of U after FeS depletion may be due to (1) the formation of U(VI) surface coatings during oxygen scavenging, or (2) the production of the Fe(III) oxides that serve as additional oxidants for UO_2 once the FeS is depleted.

To investigate the first hypothesis, solid samples of U were collected during dissolution reaction in the presence of FeS. The Fourier transforms of the sample (Figure 4.8) showed that UO_2 was the primary U(IV) solid phase retained in the CSTR when FeS was present, without significant accumulation of U(VI) species within the solid phases (<10% of the total). The fitting of data shows the presence of a U-O path at ~1.9 Å, characteristic of UO_2 phase. [This value is phase-shifted by ΔR; the corresponding phase-shift corrected U-O interatomic distance (R) is ~2.33 Å.] The first shell has a coordination number (CN) of 5.9, which decreased from 8 O of a crystalline UO_2. The second-shell CN is not only lower than a crystalline UO_2 with 12 U(IV) neighbors, but also decreased from earlier samples in the time series (~4.4 U). The solid phase U is comparable with biogenic uraninite samples (Singer et al., 2009; Veeramani et al., 2009) from previous studies. Thus, a surface U(VI) coating on the UO_2 core probably is not present, but the result need to be further confirmed by XPS for possible U(V) species.
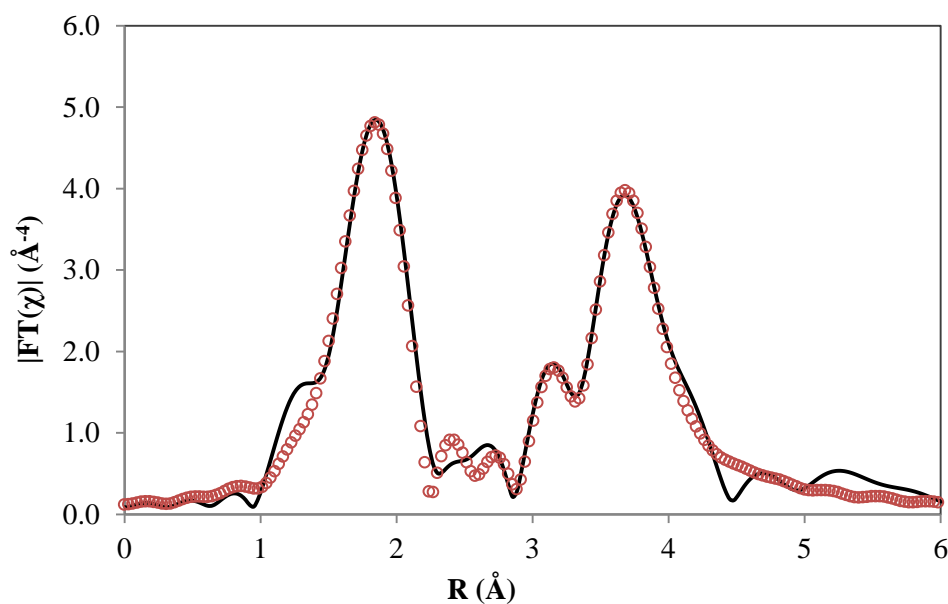

Figure 4.8. The magnitude of the Fourier transform of the $\chi(k)*k^3$ data (2.0–11 Å^{-1}) for U sample collected at 160 residence times in flow-through experiment in the presence of 18.7 mM FeS at pH 7.1 (the line represents smoothed data: while the dots represent the numerical fits).

To determine the role of Fe(III) oxides as oxidants for UO_2, Fe(III) products were first obtained from FeS oxidation with 1.8 mg/L DO, pH 7 groundwater conditions. The oxidation

products (goethite, lepidocrocite, and elemental sulfur) then reacted with synthetic UO_2 particles in the CSTR system. The dissolution profiles of UO_2 show almost identical $[U]_{diss}$ trends in the presence or absence of Fe(III) oxides (Figure 4.9), suggesting little impact of Fe(III) on the UO_2 oxidative dissolution rate when oxygen was the dominant oxidant. The results are consistent with previous research (Ginder-Vogel et al., 2010) that indicated three orders of magnitude slower rate of UO_2 dissolution by ferrihydrite than by oxygen.
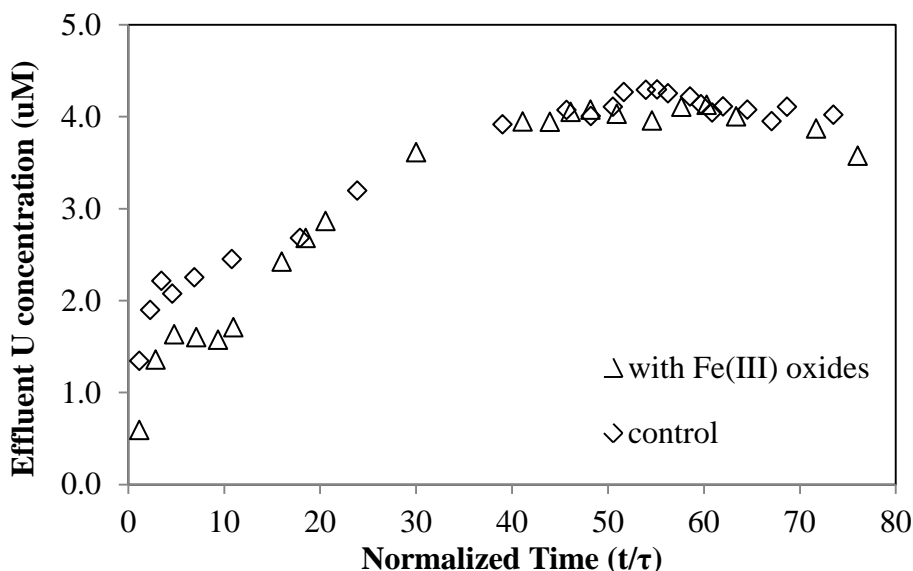

Figure 4.9. The total dissolved U release profiles in the presence and absence of Fe(III) oxides under pH =7 and 1.8 mg/L DO artificial groundwater solution.

To study the impact of Fe(III) oxides with low DO, the UO_2 was first reacted with an anoxic solution, which was constantly sparged with nitrogen gas, and then treated with 1.8 mg/L DO groundwater solution. Figure 4.10 shows that the dissolved U concentration was about two-fold higher than in absence of Fe(III), suggesting that Fe(III) oxides enhanced the dissolution rate of UO_2 with a low oxygen concentration. After being exposed to oxic flow, the dissolved U concentration increased to the level similar to the control.

In summary for this section, UO_2 quickly dissolved after FeS was depleted due to oxidation by dissolved oxygen. Iron(III) oxides produced from FeS oxidation probably were not responsible for promoting the quick release of U(VI) into effluent solution. Although accumulation of U(VI) surface coatings on UO_2 core was not identified using EXAFS analysis, a different phase from UO_2 may form during inhibited dissolution which then controlled the solubility of U after oxygen breakthrough. The phase is currently being identified by XPS.
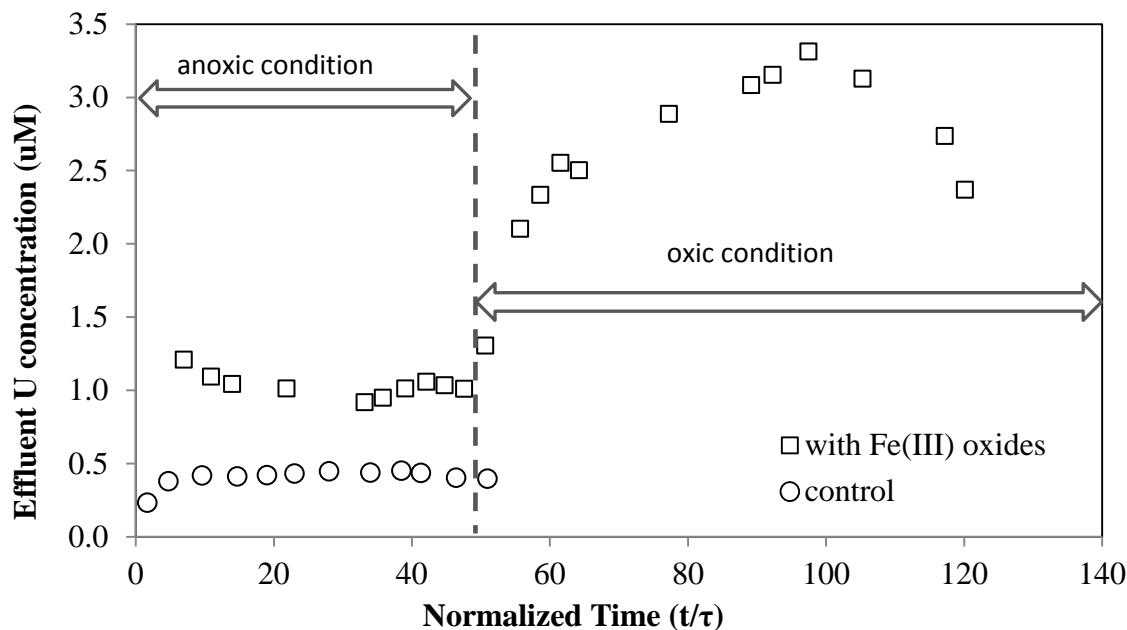
Figure 4.10. The total dissolved U release profiles in the presence and absence of Fe(III) oxides under initially anoxic conditions, then exposed to 1.8 mg/L DO artificial groundwater solution.

4.4 References

Abdelouas, A., Lutze, W., and Nuttall, H. E., 1999. Uranium Contamination in the Subsurface: Characterization and Remediation. *Reviews in Mineralogy <D>* **38**, 433-473.

Bargar, J. R., Williams, K. H., Campbell, K. M., Long, P. E., Stubbs, J. E., Suvorova, E. I., Lezama-Pacheco, J. S., Alessi, D. S., Stylo, M., Webb, S. M., Davis, J. A., Giammar, D. E., Blue, L. Y., and Bernier-Latmani, R., 2013. Uranium redox transition pathways in acetate-amended sediments. *Proceedings of the National Academy of Sciences*.

Ginder-Vogel, M., Criddle, C. S., and Fendorf, S., 2006. Thermodynamic constraints on the oxidation of biogenic UO2 by Fe(III) (hydr) oxides. *Environmental Science & Technology* **40**, 3544-3550.

Ginder-Vogel, M., Stewart, B., and Fendorf, S., 2010. Kinetic and Mechanistic Constraints on the Oxidation of Biogenic Uraninite by Ferrihydrite. *Environmental Science & Technology* **44**, 163-169.

Morgan, B. and Lahav, O., 2007. The effect of pH on the kinetics of spontaneous Fe(II) oxidation by O-2 in aqueous solution - basic principles and a simple heuristic description. *Chemosphere* **68**, 2080-2084.

Rickard, D. and Morse, J. W., 2005. Acid volatile sulfide (AVS). *Marine Chemistry* **97**, 141-197.

Sani, R. K., Peyton, B. M., Dohnalkova, A., and Amonette, J. E., 2005. Reoxidation of reduced uranium with iron(III) (hydr)oxides under sulfate-reducing conditions. *Environmental Science & Technology* **39**, 2059-2066.

Singer, D. M., Farges, F., and Brown, G. E., 2009. Biogenic nanoparticulate UO2: Synthesis, characterization, and factors affecting surface reactivity. *Geochimica Et Cosmochimica Acta* **73**, 3593-3611.

Ulrich, K. U., Ilton, E. S., Veeramani, H., Sharp, J. O., Bernier-Latmani, R., Schofield, E. J., Bargar, J. R., and Giammar, D. E., 2009. Comparative dissolution kinetics of biogenic

and chemogenic uraninite under oxidizing conditions in the presence of carbonate. *Geochimica Et Cosmochimica Acta* **73**, 6065-6083.

Veeramani, H., Schofield, E. J., Sharp, J. O., Suvorova, E. I., Ulrich, K.-U., Mehta, A., Giammar, D. E., Bargar, J. R., and Bernier-Latmani, R., 2009. Effect of Mn(II) on the Structure and Reactivity of Biogenic Uraninite. *Environmental Science & Technology* **43**, 6541-6547.

5. Column experiments on stability of UO_2 and biogenic FeS

The UM team also carried out a long-term sediment column experiment to investigate the stability of reduced U solids under oxidizing conditions in the presence or absence of biogenic iron sulfides. Specifically, the column work assessed the capacity of mackinawite to protect uraninite against oxidation during abiotic oxidant intrusion in columns packed with a bio-reduced Rifle area background sediment (RABS). The Rifle, CO site is a former processing site for U ore, now being remediated so that it can be decommissioned. The dynamics of *in-situ* U bio-remediation, in which dissolved and relatively mobile U(VI) species are reduced to insoluble U(IV) solid phases, has been extensively studied at the Rifle site (Campbell et al. 2011; Anderson et al. 2003; Yabusaki et al. 2007). Although several studies have focused on the role of microbial activity in regulating redox conditions and U speciation during oxidant intrusion into bio-reduced sediments (H.S. Moon, Komlos, and Jaffé 2009; Hee Sun Moon, Komlos, and Jaffé 2007; Myneni 2009; John Komlos et al. 2008; J. Komlos et al. 2008; N'Guessan et al. 2010; Sani et al. 2005), no study has addressed the abiotic redox controls in absence of significant microbial activity. In order to develop robust models of U transport in sediments undergoing redox fluctuations, the role of abiotic processes needs to be delineated and was, therefore, a primary focus of this study.

Reduced U phases, produced in bioreducing zones, may be exposed to periodic oxidant intrusion in the subsurface. If bioreduced U is reoxidized and mobilized in these circumstances, it diminishes the effectiveness of this approach. Oxygen is one potential oxidant capable of migrating into U bioremediation zones from oxic groundwater sources or rainwater infiltration. As shown in Section 3 above, dissolved oxygen can rapidly oxidize UO_2 in well-mixed batch and flow-through reactor systems when no sediment is present (Bi et al. 2013; Bi and Hayes 2014). Abiotic U oxidation by nitrite, a denitrification intermediate, is another potentially important U oxidation remobilization pathway. Given the co-occurrence of nitrate and U in groundwater (Riley and Zachara 1992), the potential for nitrite to oxidize reduced U also warrants attention. Nitrite has benn reported to oxidize and remobilized reduce U (IV) species in batch reactor laboratory experiments (Senko et al. 2002; Senko et al. 2005; Finneran, Housewright, and Lovley 2002). Hence, in this column study, the potential of both nitrite and oxygen to serve as abiotic oxidants of reduced U have been studied.

For this study, we first bio-reduced RABS by amending the natural mixed microbial community present with acetate using two flow-through sediment columns in parallel: One had sulfate reduction due to addition of sulfate to the influent, while the other lacked sulfate and thus was devoid of sulfate reduction. In the column undergoing sulfate reduction, biogenic iron sulfide formed, while in the other column reduced iron phases formed, but no iron sulfide was present. After 65 days, the sediments were removed from the columns, and synthetic uraninite was added. The uraninite-bearing sediments were then gamma sterilized to significantly reduce microbial activity, placed back in columns, and then subjected to a short anaerobic stabilization period in which anoxic influent was maintained for 6 days. Subsequently, both columns were exposed to nitrite to assess its potential for oxidation based on monitoring for the breakthrough of U(VI) in the column effluent. Nitrite was then replaced with dissolved oxygen in both columns, and U(VI) was again monitored to determine the extent of uraninite oxidation by oxygen. The role of iron sulfide in protecting uraninite against oxidation was directly evaluated by comparing the results from column with versus the one without iron sulfide.

Overall, the primary objectives of this study were to assess (1) the capacity of biogenic iron sulfides to protect uraninite from abiotic oxidation by nitrite and dissolved oxygen, and (2) the abiotic oxidation potential of nitrite and oxygen on uraninite in bio-reduced sediment packed in column reactors.

5.1 Bioreduction

For the bioreduction phase, two 4.8-cm diameter, 15-cm long glass columns were packed with RABS mixed with a seed sample of fresh microbially active sediment from the Rifle site. Artificial groundwater (AGW) was then pumped through the packed sediment columns at a constant flow rate of 0.5 ml/min. The AGW contained 3 mM acetate to stimulate microbial growth, plus bicarbonate (8 mM), calcium (1 mM), magnesium (1 mM), sodium (8 mM), potassium (0.27 mM), and chloride (4.45 mM), but no uranium or iron. One of the two columns, the BRS+ column (bioreduction, with sulfate), was supplemented with 7 mM sodium sulfate for the duration of reduction.

To verify that bioreduction was taking place, Fe(II), sulfate, and sulfide concentrations were monitored in the effluent (Figure 5.1). At day 5, Fe (II) breakthrough occurred in both columns, indicating the onset of iron reduction (Figure 5.1.A). A subsequent sharp drop in effluent Fe(II)

in the sulfate-fed column (BRS+) at day 30 coincided with the onset of sulfate reduction, as indicated by the consumption of sulfate (Figure 5.1.B) and the release of sulfide (Figure 5.1.C). Simultaneous sulfate and iron reduction caused precipitation of iron sulfide minerals, resulting in a black-colored, iron sulfide-bearing sediment in the sulfide rich BRS+ column, while the sulfide devoid BRS- column remained brown. The biogenic iron-sulfide precipitates in the BRS+ column were identified as mackinawite by comparative EXAFS analysis (data not shown).
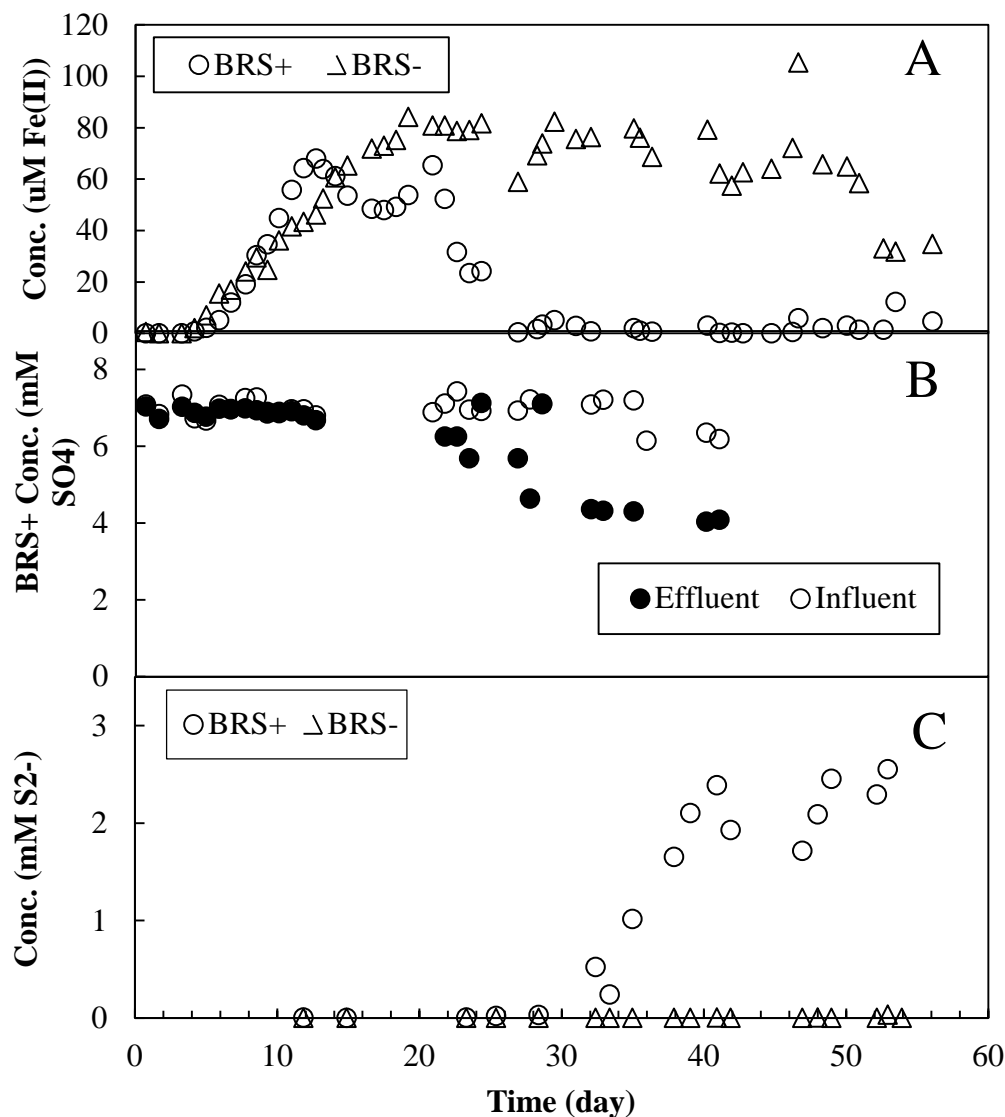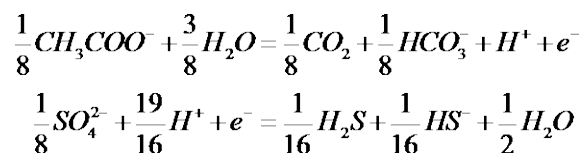

Figure 5.1. Effluent concentration of ferrous iron indicates the onset of iron reduction at day 5 and the loss of ferrous ion between day 25 and 30 indicates the onset of sulfate reduction (A), as does the consumption of sulfate during the same period (B). The increase in the effluent concentration of sulfide starting at day 25 further indicates the onset of microbial sulfate reduction (C).

Once sulfate reduction was fully under way (by day 30) in the BRS+ column, ~3 mM sulfate was continuously consumed, along with ~3 mM acetate (data not shown). This 1:1 stoichiometry agrees with the two half reactions for microbial sulfate reduction using acetate as an electron donor as follows:

$$\frac{1}{8}CH_3COO^- + \frac{3}{8}H_2O = \frac{1}{8}CO_2 + \frac{1}{8}HCO_3^- + H^+ + e^-$$

$$\frac{1}{8}SO_4^{2-} + \frac{19}{16}H^+ + e^- = \frac{1}{16}H_2S + \frac{1}{16}HS^- + \frac{1}{2}H_2O$$

5.2 Oxidation

To observe the abiotic response of uraninite to oxidants in the column studies, after 65 days of acetate-stimulated bio-reduction, the bio-reduced sediments were removed from the columns, thoroughly mixed with synthetic uraninite, and then sterilized with 5 Mrad gamma radiation at the University of Michigan Phoenix Memorial Lab Co-60 source over a 15 hour period. Once irradiated, the sediments were re-packed back into the original glass columns, which had been sterilized by autoclaving. Anoxic AGW flow was initiated immediately after packing and continued for 6 days. The oxidation phase was then initiated by introducing 0.53 mM (24.4 mg/L) nitrite in the AGW at day 6. Nitrite-containing influent was discontinued at day 15.5, when 0.27 mM (8.5 mg/L) dissolved oxygen was introduced and maintained in the influent for the duration of the experiment (10 more days). The AGW influent was carbonate buffered to circumneutral pH by continuous gas purging with 5% CO_2/gas mixture in a 23-L glass carboy. During anoxic flow and nitrite addition, a 5% CO_2/95% N_2 gas mixture was used; for oxygenated flow, a 5% CO_2/95% air mixture was used. During the oxidation phase, effluent samples were monitored for dissolved Fe(II), sulfide, sulfate, thiosulfate, dissolved oxygen (DO), nitrite, and U(VI) to assess whether oxidation reactions were taking place between the oxidants, nitrite and DO, and the uraninite and Fe(II) solid phases present in the sediment. Tetrachloroethylene extraction of the sediments for elemental sulfur (S^0) was also performed. Previous work by Burton et al. (2009) and Bi et al. (2012) showed that elemental sulfur is the primary sulfur abiotic oxidation product when mackinawite reacts with oxygen.

During the 6-day anoxic stabilization period (prior to addition of nitrite), the average uranium concentrations in the effluents of the BRS+ and BRS- columns were low, 0.16 µM ± 0.12 µM and 0.29 µM ± 0.07 µM, respectively (Figure 5.2). Thus, U oxidation and mobilization were

minimal before the oxidants were introduced. Also during this anoxic period, the influent dissolved oxygen concentration was less than 0.04 µM (Figure 5.3), with detectable Fe(II) (Figure 5.4) and sulfide (Figure 5.5) measured in the effluent of the BRS+ column indicating anoxic conditions.
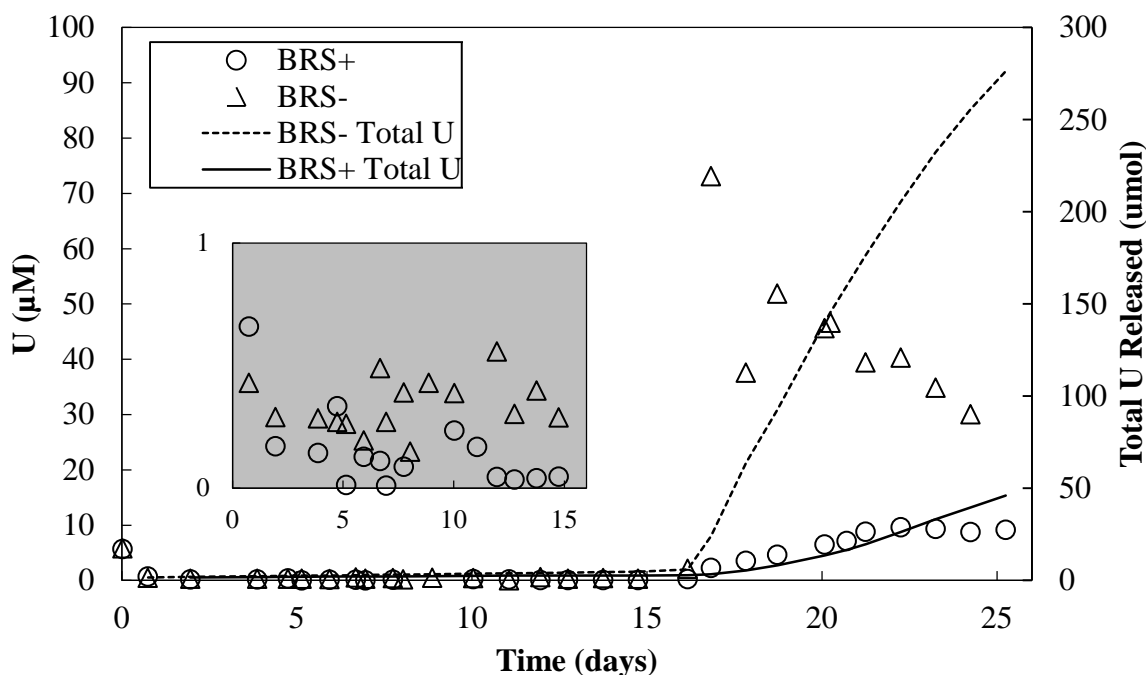

Figure 5.2. Effluent uranium concentrations (open symbols) during the oxidation phase, with cumulative Total U indicated by the lines. Nitrite (0.53 mM) was introduced at day 6 and was replaced by dissolved oxygen (0.27 mM) on day 15.5. The grey insert shows an expanded view of first 16 days of data.

The nitrite oxidation phase began on day 6. As shown in Figure 5.2, nitrite did not significantly oxidize uraninite over the entire nitrite oxidation segment (days 6 through 15.5); no significant U breakthrough was observed. During this phase, the U effluent concentration stayed low, between 0.14 and 0.56 µM, with an average of 0.37 µM ± 0.12 µM (one standard deviation) for the BRS- column, and between 0.01 and 0.24 µM, with an average of 0.09 µM ± 0.07 µM (one standard deviation) for U in the BRS+ column. The relatively large standard deviations of the averages indicated that nitrite was not significantly inducing U release compared to the anoxic flow condition. Also, the effluent U concentrations during nitrite flow were low in comparison to those observed during oxygenated flow, as discussed below.
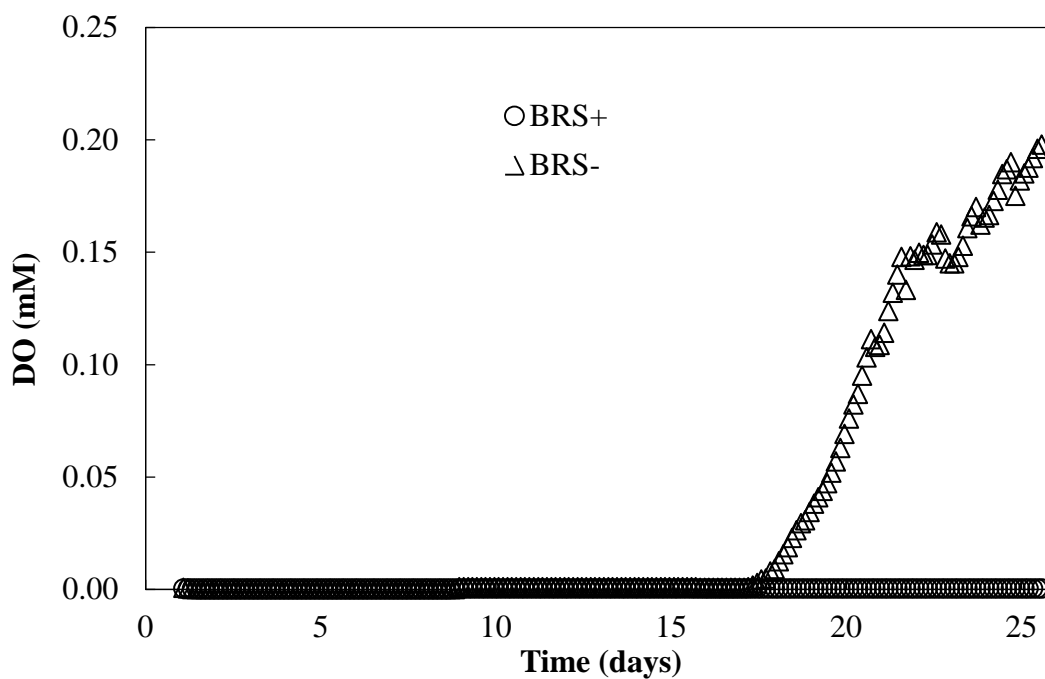
Figure 5.3. Dissolved oxygen remained below 1 uM in the effluent of both columns until day 16 when breakthrough was observed in the BRS- column.
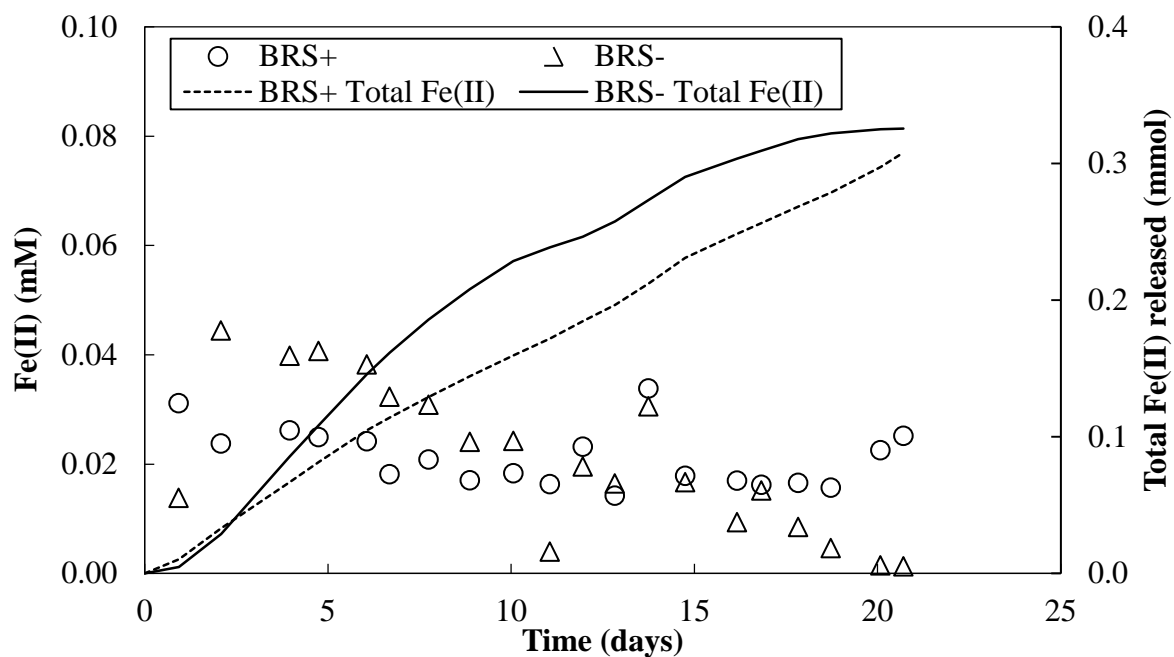

Figure 5.4. Effluent [Fe(II)] and the cumulative total amount of Fe(II) leached over the course of the oxidation phase for both columns.
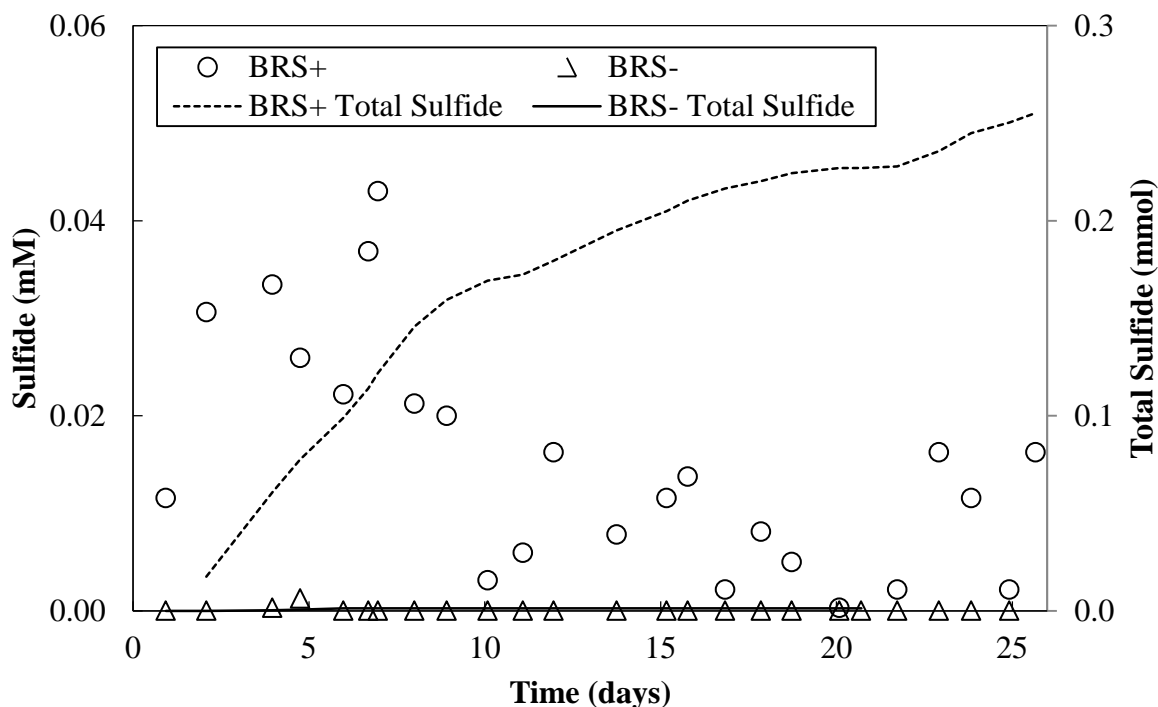
Figure 5.5. No sulfide was observed in the effluent of the BRS- column; up to 0.03 mM (~1 mg/L) sulfide was measured in the effluent of the BRS+ column. Sulfide concentrations in general began decreasing after the introduction of nitrite around day 7.

The nitrite concentration, compared to uranium in the effluent, was more significantly lowered, especially in the BRS+ column. This decrease in nitrite concentration was most likely linked to the abiotic nitrite reduction by other reducing species in the sediment. To accentuate nitrite reduction, the influent flow was interrupted for approximately 12 hours on days 11 and 12 in the BRS+ and BRS- columns, respectively. After this flow interruption, 0.3 mM nitrite was consumed (Figure 5.6), but the uranium effluent concentration remained consistently low (< 0.5 μM, Figure 5.2), indicating that U(IV) was not significantly oxidized, and, therefore, not directly linked to nitrite reduction. Approximately 0.3 mM nitrite was consumed during the flow stoppage in both columns, compared to their effluent controls (Figure 5.6), with Fe(II) and sulfide the most likely reductants. Since, in the BRS+ column, no effluent sulfate was measured and sulfur extractions of the sediment revealed significant elemental sulfur content after oxidation, the primary oxidation product of nitrite reduction by sulfide was likely S^0 (elemental sulfur).
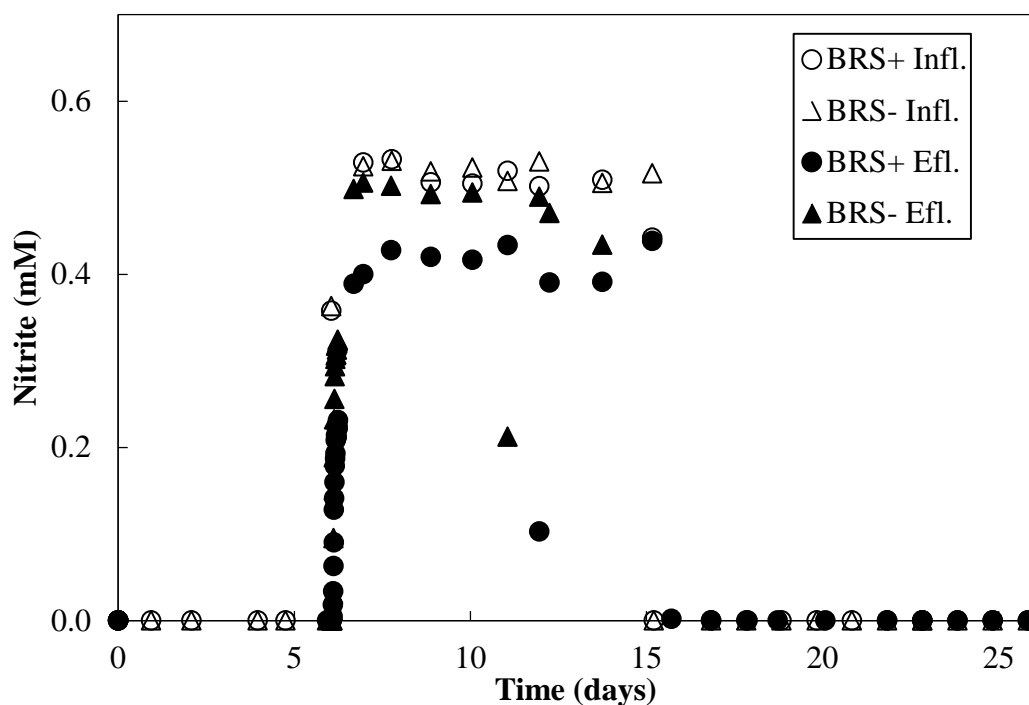
Figure 5.6. Influent (open symbols) and effluent (closed symbols) nitrite concentration for BRS+ and BRS- columns, showing the initiation of nitrite amended flow at day 6, consumption of nitrite during the nitrite flow segment, and the discontinuation of nitrite amendment at day 15.5.

The introduction of dissolved oxygen on day 16 immediately induced mobilization of U in both columns, with a faster release of U observed in the BRS- column (Figure 5.2). The uranium concentration in the BRS+ column continued to increase until day 21, after which a plateau was reached. In contrast, the uranium concentration in the BRS- column peaked after just 2 days of oxygenated flow and remained elevated with the average concentration during oxidative flow of 43 µM, approximately 6 times greater than the average in the BRS+ column (7 µM) over the same time period.
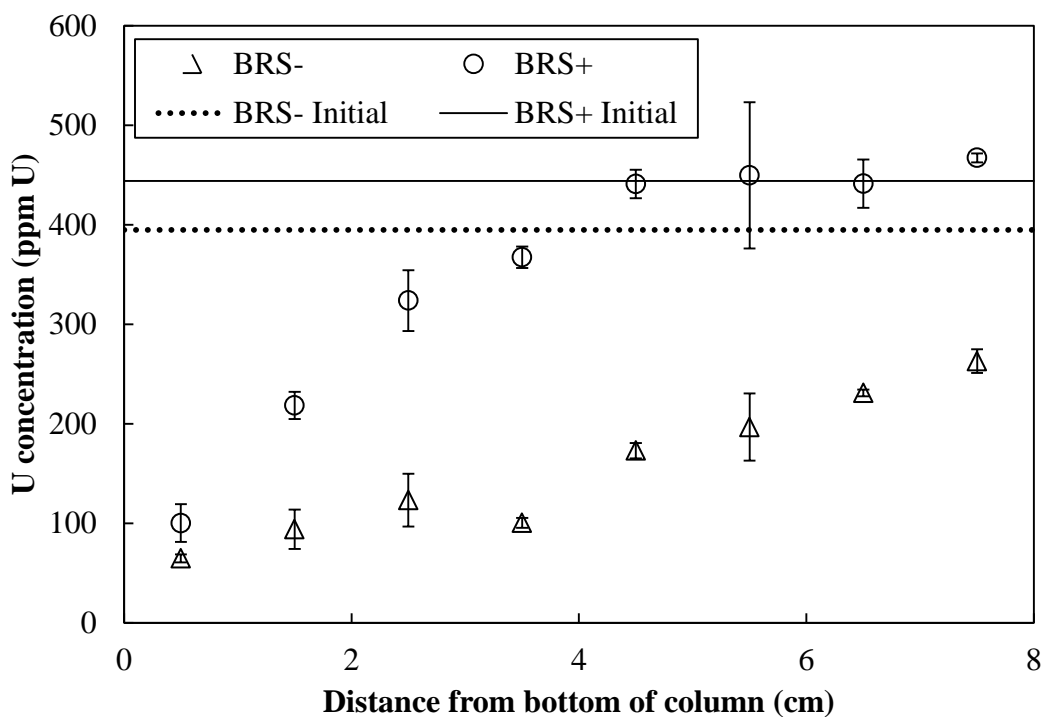
Figure 5.7. Hot nitric acid digestion of sediment samples taken at 1-cm increments along the lengths of both columns show that the BRS- column lost more (79%) of its original uranium than the BRS+ column which lost 39% of its original uranium added as uraninite.

Sediment U extractions demonstrate the presence of mackinawite inhibited uraninite oxidation (Figure 5.7). For example, at the end of the oxidation phase, the BRS+ and BRS- columns retained approximately 61% and 21%, respectively, relative to original uranium content (~400 µg/g and ~440 µg/g, respectively). This comparison illustrates the superior oxygen scavenging capacity of the bioreduced iron sulfide minerals formed in the SBR+ column compared to bioreduced Fe(II) solid phases in the SBR- column. The lack of oxygen breakthrough in the BRS+ column in combination with immediate oxygen breakthrough in the BRS- column (Figure 5.3) demonstrated the significant capacity of mackinawite to maintain reducing conditions during oxygen intrusion and also that the reduced sediment lacking mackinawite had little capacity to take up dissolved oxygen. Dissolved oxygen breakthrough did not occur at all in the BRS+ column over the course of this experiment, although a sulfide oxidation front was clearly visible in the BRS+ column, as evidenced by a color change from

black to tan taking place as the oxidation front moved from the influent end toward the effluent end of the column with time.

The lack of sulfide oxidation to sulfate in the BRS+ column and immediate breakthrough of dissolved oxygen in the BRS- column indicate minimal microbial activity during the oxidation phase. Further, sulfur extractions of the sediments showed elemental sulfur (S^0) as the primary sulfide product from mackinawite oxidation, with higher concentrations near the influent end of the BRS+ column (data not shown). Previously, Burton et al. (2009) found elemental sulfur was the primary product of abiotic sulfide oxidation of sediments, while microbial oxidation led to sulfate production, confirming that sulfur-oxidizing microbes were not likely active in our system. Dissolved oxygen breakthrough also began almost immediately in the BRS- column, supporting that minimal microbial activity in the columns occurred during the abiotic oxidation phase (Figure 5.3). In previous column studies (unpublished data), we found microbially active Rifle sediments consumed significant amounts of dissolved oxygen, delaying oxygen breakthrough for more than 10 days. Moon et al. (2007) observed a 20-day delay in dissolved oxygen breakthrough in a column study using a microbially active, bio-reduced sediment. The immediate dissolved oxygen breakthrough observed in our study thus demonstrates that oxygen-consuming microbes, if present, were not active. Taken together, these results indicate that gamma irradiation for sterilization of the sediments was effective, allowing abiotic conditions to prevail over the course of the oxidation phase.

In summary, naturally occurring sulfate- and iron-reducing bacteria in the RABS produced sulfide and ferrous iron, leading to the formation of mackinawite and other reduced-iron phases. After gamma irradiation, the sediment containing mackinawite significantly slowed the abiotic uraninite oxidation and mobilization of U compared to the sediment devoid of mackinawite. Under these abiotic conditions, oxygen, but not nitrite, rapidly oxidized uraninite causing U mobilization. Nitrite, however was not a significant abiotic oxidant for uraninite, although nitrite reduction by Fe(II) and sulfide was observed.

5.3 References

Anderson, Robert T., Helen A. Vrionis, Irene Ortiz-Bernad, Charles T. Resch, Philip E. Long, Richard Dayvault, Ken Karp, et al. 2003. "Stimulating the In Situ Activity of Geobacter Species To Remove Uranium from the Groundwater of a Uranium-Contaminated Aquifer." *Applied and Environmental Microbiology* 69 (10) (October 1): 5884–5891. doi:10.1128/AEM.69.10.5884-5891.2003.

Burton, E.D., R.T. Bush, L.A. Sullivan et al. "Iron-Monosulfide Oxidation in Natural Sediments: Resolving Microbially Mediated S Transformations Using XANES, Electron Microscopy, and Selective Extractions." *Environmental Science & Technology*, 43 (9) 3128-3143, 2009.

Bi, Y., and K. F. Hayes. 2014. "Nano-FeS Inhibits UO2 Reoxidation Under Varied Oxic Conditions." *Environmental Science & Technology* 48 (1) (January 7): 632–640. doi:10.1021/es4043353.

Bi, Yuqiang, S. P. Hyun, R. K. Kukkadapu, and K. F. Hayes. 2013. "Oxidative Dissolution of UO2 in a Simulated Groundwater Containing Synthetic Nanocrystalline Mackinawite." *Geochimica Et Cosmochimica Acta* 102 (February 1): 175–190. doi:10.1016/j.gca.2012.10.032.

Campbell, K. M., H. Veeramani, K.-U. Ulrich, L. Y. Blue, D. E. Giammar, R. Bernier-Latmani, J. E. Stubbs, et al. 2011. "Oxidative Dissolution of Biogenic Uraninite in Groundwater at Old Rifle, CO." *Environmental Science & Technology* 45 (20) (October 15): 8748–8754. doi:10.1021/es200482f.

Finneran, K. T., Meghan, E. Housewright, and D. R. Lovley. 2002. "Multiple Influences of Nitrate on Uranium Solubility During Bioremediation of Uranium-contaminated Subsurface Sediments." *Environmental Microbiology* 4 (9): 510–516. doi:10.1046/j.1462-2920.2002.00317.x.

Komlos, J., B. Mishra, A. Lanzirotti, S. Myneni, and P. Jaffé. 2008. "Real–Time Speciation of Uranium During Active Bioremediation and Reoxidation." *Journal of Environmental Engineering* 134 (2): 78–86. doi:10.1061/(ASCE)0733-9372(2008)134:2(78).

Komlos, John, Aaron Peacock, Ravi K. Kukkadapu, and Peter R. Jaffé. 2008. "Long-term Dynamics of Uranium Reduction/reoxidation Under Low Sulfate Conditions." *Geochimica Et Cosmochimica Acta* 72 (15) (August 1): 3603–3615. doi:10.1016/j.gca.2008.05.040.

Moon, H.S., J. Komlos, and P.R. Jaffé. 2009. "Biogenic U(IV) Oxidation by Dissolved Oxygen and Nitrate in Sediment After Prolonged U(VI)/Fe(III)/SO42- Reduction." *Journal of Contaminant Hydrology* 105 (1-2) (February 27): 18–27. doi:10.1016/j.jconhyd.2008.10.014.

Moon, Hee Sun, John Komlos, and Peter R. Jaffé. 2007. "Uranium Reoxidation in Previously Bioreduced Sediment by Dissolved Oxygen and Nitrate." *Environmental Science & Technology* 41 (13) (July 1): 4587–4592. doi:10.1021/es063063b.

Myneni, Peter R Jaffe Satish. 2009. "Reduction and Reoxidation of Soils During and After Uranium Bioremediation; Implications for Long Term Uraninite Stability and Bioremediation Scheme Implementation." http://www.osti.gov/bridge/servlets/purl/963722-SNpoSD/.

N'Guessan, Adeola Lucie, Hee Sun Moon, Aaron D Peacock, Hui Tan, Malavika Sinha, Philip E Long, and Peter R Jaffé. 2010. "Postbiostimulation Microbial Community Structure

Changes That Control the Reoxidation of Uranium." *FEMS Microbiology Ecology* 74 (1) (October 1): 184–195. doi:10.1111/j.1574-6941.2010.00933.x.

Riley, R. G., and J. M. Zachara. 1992. "Chemical Contaminants on Doe Lands and Selection of Contaminant Mixtures for Subsurface Science Research". DOE/ER--0547T. Pacific Northwest Lab., Richland, WA (United States). http://www.osti.gov/energycitations/product.biblio.jsp?osti_id=10147081.

Sani, Rajesh K., Brent M. Peyton, Alice Dohnalkova, and James E. Amonette. 2005. "Reoxidation of Reduced Uranium with Iron(III) (Hydr)Oxides Under Sulfate-Reducing Conditions." *Environmental Science & Technology* 39 (7) (April 1): 2059–2066. doi:10.1021/es0494297.

Senko, John M., Jonathan D. Istok, Joseph M. Suflita, and Lee R. Krumholz. 2002. "In-Situ Evidence for Uranium Immobilization and Remobilization." *Environmental Science & Technology* 36 (7) (April 1): 1491–1496. doi:10.1021/es011240x.

Senko, John M., Yasser Mohamed, Thomas A. Dewers, and Lee R. Krumholz. 2005. "Role for Fe(III) Minerals in Nitrate-Dependent Microbial U(IV) Oxidation." *Environmental Science & Technology* 39 (8) (April 1): 2529–2536. doi:10.1021/es048906i.

Yabusaki, Steven B., Yilin Fang, Philip E. Long, Charles T. Resch, Aaron D. Peacock, John Komlos, Peter R. Jaffe, et al. 2007. "Uranium Removal from Groundwater via in Situ Biostimulation: Field-scale Modeling of Transport and Biological Processes." *Journal of Contaminant Hydrology* 93 (1-4) (August 15): 216–235. doi:10.1016/j.jconhyd.2007.02.005.

6. Summary of Publications and Presentations from the Project:

6.1 Peer-reviewed publications

1. Bi, Y., Hyun, S. P., Kukkadapu, R. K., Hayes, K. F. Oxidative dissolution of UO_2 in a simulated groundwater containing synthetic nanocrystalline mackinawite. *Geochimica et Cosmochimica Acta* 2013, 102, 175-190. [This manuscript corresponds to Section 4.1]
2. Bi, Y., and Hayes, K. F. Nano-FeS Inhibits UO_2 Reoxidation under Varied Oxic Conditions. *Environ. Sci. Technol.* 2014, 48, 632-640. [This manuscript corresponds to Section 4.2]
3. Bi, Y., and Hayes, K. F. Labile U(VI) phases formed during inhibited UO_2 dissolution in the presence of iron sulfide. *Environ. Sci. Technol.* 2013, in progress [This manuscript corresponds to Section 4.3]
4. Carpenter, J. Bi, Y., Hyun, S.P., Clancy, T.M., and Hayes, K.F., "Influence of iron sulfide minerals on oxidation of reduced uranium solids in natural sediments," *Environmental Science and Technology*, 2013, in progress [This manuscript corresponds to Section 5]
5. Hyun, S.P., Davis, J.A., Sun, K., and Hayes, K.F., "U(VI) reduction by iron(II) monosulfide mackinawite," *Environmental Science and Technology*, 46, 3369-3376, 2012. [This manuscript corresponds to Section 3.1]
6. Hyun, S.P., and Hayes, K.F., "Surface complexation modeling of U(VI) adsorption by aquifer sediments from a former mill tailings site at Rifle, Colorado," *Environmental Science and Technology*, 43, 9368-9373, 2009.
7. Hyun, S.P., Davis, J.A., and Hayes, K.F., "Abiotic U(VI) reduction by aqueous sulfide," *Environmental Science and Technology*, in review, 2013 [This manuscript corresponds to Section 3.2].
8. Zhou, C., Rittmann, B.E., Hayes, K.F., and Vannela, R., "Effect of growth conditions on formation and characteristics of biogenic iron-sulfide solids by *Desulfovibrio vulgaris*," Applied Environmental Microbiology, in review, 2013 [This manuscript corresponds to Section 2.1]
9. Zhou, C., Rittmann, B.E., Hayes, K.F., and Vannela, R., "Effect of iron source on Desulfovibrio *vulgaris* growth and FeS solid formation, "Environmental Science and Technology, in progress, 2013 [This manuscript corresponds to Section 2.2]
10. Zhou, C., Rittmann, B.E., Hayes, K.F., and Vannela, R., "*Desulfovibrio vulgaris* shows distinct sulfate/Fe(III) reduction patterns and biogenic FeS characteristics when the electron donor is pyruvate," Environmental Science and Technology, in progress, 2013 [This manuscript corresponds to Section 2.2]

6.2 National and International Conference Presentations

1. Bi, Y., and Hayes, K.F., Enhanced Stability and Inhibited Dissolution of Uraninite by Nanoparticulate Iron Sulfide under Oxic Conditions, oral presentation at Goldschmidt 2013, Florence, Italy, August 25-31, 2013.
2. Bi, Y., Carpenter, J.R., and Hayes, K.F., Impact of iron sulfide minerals on UO_2 reoxidation in groundwater, presented at the 245th American Chemical Society National Meeting, New Orleans, LA, April 7-11, 2013.

3. Bi, Y., Hyun, S.P., and Hayes, K.F., Inhibited Oxidation of Synthetic Uraninite by Mackinawite, presented at the U.S. Department of Energy Subsurface Biogeochemical Research Annual Meeting, Washington D.C., April 30- May 2, 2012.
4. Bi, Y., Carpenter, J.R., Hyun, S.P., and Hayes, K.F., Inhibited Oxidation of Synthetic Uraninite in the Presence of FeS and the Implication to U Remediation, presented at the 243th American Chemical Society National Meeting, San Diego, CA, March 25-29, 2012.
5. Bi, Y., Hyun, S.P., and Hayes, K.F., The Double Role of Iron Sulfide Minerals in Remediation of Uranium-contaminated Groundwater, presented at the Engineering Graduate Symposium, University of Michigan, Ann Arbor, November 11, 2011.
6. Bi, Y., Hyun, S.P., and Hayes, K.F., Dissolution of Uraninite by Dissolved Oxygen under Simulated Groundwater Conditions in the Presence of Mackinawite (FeS), presented at the 241th American Chemical Society National Meeting, Anaheim, CA, March 27-31, 2011.
7. Bi, Y., Hyun, S.P., and Hayes, K.F., Oxidative Dissolution of Uraninite in the Presence of Mackinawite (FeS) under Simulated Groundwater Conditions, poster presented at the 2010 American Geophysical Union Fall Meeting, San Francisco, CA, December, 13-17, 2010.
8. Bi, Y., Hyun, S.P., and Hayes, K.F., Oxidative Dissolution of Mackinawite by Dissolved Oxygen in the Presence of Synthetic Uraninite, poster presented at the 239th American Chemical Society National Meeting, San Francisco, CA, March 21-25, 2010.
9. Carpenter, J.R., Hayes, K.F. Influence of iron sulfide minerals on oxidation of reduced uranium solids in natural sediments, presented at the 242nd ACS National Meeting, Denver, CO, August 28-September 1 2011.
10. Carpenter, J.R., Hyun, S.P., Hayes, K.F., Synchrotron X-ray characterization of mackinawite and uraninite relevant to bio-remediation of groundwater contaminated with uranium, poster presented at the 2010 American Geophysical Union Fall Meeting, San Francisco, CA, December. 13-17, 2010.
11. Hayes, K.F., (invited), Bi, Y., Carpenter, J.C., Hyun, S.P., and Kukkadapu, R., "Column and Batch Reactor Studies of the Inhibition of UO_2 oxidative dissolution by synthetic FeS," Uranium biogeochemistry: transformations and applications," International Workshop, Monte Verita, Ascona Switzerland, March 11-16, 2012.
12. Hayes, K.F., Bi, Y., Carpenter, J.R., Rittmann B.E., Zhou, C., and Vannela, R., Inhibited Oxidation of Synthetic Uraninite by Mackinawite, presented at the U.S. Department of Energy Subsurface Biogeochemical Research Annual Meeting, Potomac, MD, May 14-15, 2013.
13. Hyun, S.P. (invited), Davis, J.A., and Hayes, K.F., "Uranium (VI) reactions with aqueous and ferrous sulfide," in special symposium on Redox Transformations of Metals in Sediments at Molecular and Pore Scales, 243rd National Meeting of American Chemical Society, San Diego CA, March 25-29, 2012.
14. Hyun, S.P., Davis, J.A., and Hayes, K.F., "Abiotic Reduction of U(VI) by Dissolved Sulfide," American Geophysical Union Fall Meeting, December 13-17, San Francisco, CA, 2010.
15. Hyun, S.P., Bi, Y., Kukkadapu, R., Sun, K., Bargar, J., and Hayes, K.F., "Iron sulfide protection of reduced U against oxidation by dissolved oxygen," in Aquatic Redox

Chemistry Symposium in Honor of Donald L. Macalady, 239th ACS National Meeting, San Francisco, CA, March 21-25, 2010.

16. Hyun, S.P., Hayes, K.F., and Davis, J.A., "Surface Complexation Modeling of U(VI) Adsorption by an Aquifer Sediment from a Former Mill-Tailings Site at Rifle, CO," 237th ACS National Meeting, Salt Lake City, UT, March 22-26, 2009.

17. Zhou, C., Vannela, R., Rittmann, B.E., Clancy, T., Upadhyaya, G., and Hayes, K.F., Investigating the versatile contributions of a *Desulfovibrio vulgaris* strain, a sulfate-reducing bacterium, to U(VI) bioremediation, poster presented at the U.S. Department of Energy Subsurface Biogeochemical Research Annual Meeting, Washington D.C., April 26 - 28, 2011.

18. Zhou, C., Vannela, R., and Rittmann, B.E., Investigating the versatile contributions of *Desulfovibrio vulgaris* strain, a sulfate-reducing bacterium, to uranium bioremediation, posters presented at the 1st Graduate Research Symposium, School of Sustainable Engineering and the Built Environment, Arizona State University, Tempe, AZ, Mar 10, 2011.